Theses and Dissertations	Thesis and Dissertation Collection

1976-06

Electroexcitation of giant resonances in (60)Ni between 5 MeV and 30 MeV excitation energy

DuBois, Dorse Howard, II

Monterey, California. Naval Postgraduate School

http://hdl.handle.net/10945/17745

ELECTROEXCITATION
OF GIANT RESONANCES IN ^{60}Ni
BETWEEN 5 MeV AND 30 MeV
EXCITATION ENERGY

Dorse Howard DuBois

NAVAL POSTGRADUATE SCHOOL
Monterey, California

THESIS

ELECTROEXCITATION

OF GIANT RESONANCES IN ^{60}Ni

BETWEEN 5 MeV AND 30 MeV

EXCITATION ENERGY

by

Dorse Howard DuBois II

and

George Macnider Bates

June 1976

Thesis Advisors: E.B. Dally, W.R. Pitthan

REPORT DOCUMENTATION PAGE		READ INSTRUCTIONS BEFORE COMPLETING FORM
1. REPORT NUMBER	2. GOVT ACCESSION NO.	3. RECIPIENT'S CATALOG NUMBER
4. TITLE (and Subtitle) Electroexcitation of Giant Resonances in ^{60}Ni Between 5 MeV and 30 MeV Excitation Energy		5. TYPE OF REPORT & PERIOD COVERED Master's Thesis; June 1976
		6. PERFORMING ORG. REPORT NUMBER
7. AUTHOR(s) Dorse Howard DuBois II George Macnider Bates		8. CONTRACT OR GRANT NUMBER(s)
9. PERFORMING ORGANIZATION NAME AND ADDRESS Naval Postgraduate School Monterey, California 93940		10. PROGRAM ELEMENT, PROJECT, TASK AREA & WORK UNIT NUMBERS
11. CONTROLLING OFFICE NAME AND ADDRESS Naval Postgraduate School Monterey, California 93940		12. REPORT DATE June 1976
		13. NUMBER OF PAGES 76
14. MONITORING AGENCY NAME & ADDRESS(If different from Controlling Office)		15. SECURITY CLASS. (of this report) Unclassified
		15a. DECLASSIFICATION/DOWNGRADING SCHEDULE

16. DISTRIBUTION STATEMENT (of this Report)

Approved for public release; distribution unlimited.

17. DISTRIBUTION STATEMENT (of the abstract entered in Block 20, if different from Report)

18. SUPPLEMENTARY NOTES

19. KEY WORDS (Continue on reverse side if necessary and identify by block number)

^{60}Nickel, inelastic electron scattering, giant resonances, multipole transitions, nuclear resonances, nuclear transitions, LINAC, line shape fitting

20. ABSTRACT (Continue on reverse side if necessary and identify by block number)

Giant multipole resonances and bound states above 6 MeV in ^{60}Ni were studied with inelastic scattering of electrons at 102 MeV incident energy and scattering angles of 60, 75, 90, and 105 degrees. In the energy interval from 5 MeV to 40 MeV

DD $_{1\ JAN\ 73}^{FORM}$ 1473 EDITION OF 1 NOV 65 IS OBSOLETE
(Page 1) S/N 0102-014-6601 |

(20. ABSTRACT   Continued)

excitation energy, ten states and resonances were observed of

which only those below 7 MeV and those at 16.5 and 18.5

had been previously reported. Reduced transition probabilities

were calculated, and multipolarity assignments were made. The

ten transitions were observed at excitation energies of

6.1 (E3,E2), 7.0 (E3,M2), 7.6 (E2,E3,M2), 8.4 (E2,E0),

9.9 (E1), 11.8 (E2,E0), 12.9 (E3,M2), 15.0 (E4), 16.5 (E2,E0),

and 18.5 (E1) MeV.

The E4 resonance at 15.0 MeV was previously unreported.

The E2 resonance at 16.5 MeV reported in (α,α') work and the

E1 resonance at 18.5 MeV from (γ,n) were confirmed.

Electroexcitation

of Giant Resonances in ^{60}Ni

Between 5 MeV and 30 MeV

Excitation Energy

by

Dorse Howard DuBois II
Lieutenant Commander, United States Navy
B.S., United States Naval Academy, 1961

and

George Macnider Bates
Lieutenant Commander, United States Navy
B.S., United States Naval Academy, 1966

Submitted in partial fulfillment of the
requirements for the degree of

MASTER OF SCIENCE IN PHYSICS

from the

NAVAL POSTGRADUATE SCHOOL
June 1976

ABSTRACT

Giant multipole resonances and bound states above 6 MeV in ^{60}Ni were studied with inelastic scattering of electrons at 102 MeV incident energy and scattering angles of 60, 75, 90, and 105 degrees. In the energy interval from 5 MeV to 40 MeV excitation energy, ten states and resonances were observed of which only those below 7 MeV and those at 16.5 and 18.5 had been previously reported. Reduced transition probabilities were calculated, and multipolarity assignments were made. The ten transitions were observed at excitation energies of 6.1 (E3,E2), 7.0 (E3,M2), 7.6 (E2,E3,M2), 8.4 (E2,E0), 9.9 (E1), 11.8 (E2,E0), 12.9 (E3,M2), 15.0 (E4), 16.5 (E2,E0), and 18.5 (E1) MeV.

The E4 resonance at 15.0 MeV was previously unreported. The E2 resonance at 16.5 MeV reported in (α,α') work and the E1 resonance at 18.5 MeV from (γ,n) were confirmed.

TABLE OF CONTENTS

5

LIST OF TABLES

LIST OF FIGURES

I. INTRODUCTION

Giant multiple resonances can be excited with the use
of γ-rays, electrons, protons, and light nuclei in particle
accelerators. The use of electrons is a particularly good
method because the theoretical interpretation is relatively
clean-cut and independent of the effects of strong inter-
action with the nucleus being studied. Investigations of
nuclear giant resonance phenomena using the Naval Post-
graduate School 120 MeV electron linear accelerator began
in 1973. Since that time, thesis work has been done with
^{197}Au, ^{208}Pb, and ^{165}Ho [WarW 73, FerW 74, Moo 74]. Data
reduction techniques necessary to handle the large amount
of data, and to cope with the bremsstrahlung background
radiation, commonly called the radiation tail, have been
described earlier [WarW 73, FerW 74]. Using a refinement
of the computer codes and techniques described by Pitthan
[Pit 73], giant resonances of several multipolarities were
identified and comparisons were made with the experimental
evidence and results reported by other investigators
[BerF 75, YouM 76].

Previous work at the Naval Postgraduate School LINAC
on the nuclei ^{197}Au and ^{208}Pb was done at a fixed accelerator
energy but with different scattering angles to achieve
varying values of the momentum transfer. However, the
recent work done on ^{165}Ho utilized a fixed scattering angle

9

of 75 degrees and the machine energy was varied in order to
avoid difficulties from transverse contributions to the
cross section observed in other experiments [Pit 73, PitB 74].
Those investigations covered an excitation energy range from
5 MeV to 40 MeV. It was desired to extract similar informa-
tion concerning ^{60}Ni and ^{58}Ni. Again, a fixed machine energy
of 102 MeV was used and the scattering angles were changed
for this experiment. To be able to sort out transverse
contributions, it was decided to study the inelastic electron
scattering spectra of ^{60}Ni first, because the available (γ,n)
data from photoneutron experiments would facilitate inter-
pretation. Only one spectrum was taken of ^{58}Ni for
comparison purposes.

The nickel isotopes are semi-magic nuclei because they
lie in the closed P-28 proton shell.

^{58}Ni has two neutrons and ^{60}Ni has four neutrons more
than the closed neutron shell N-28. From experience with
other closed shell nuclei it can, therefore, be expected
that the continuum states are relatively structured and can
thus be disentangled from each other [PitW 71, FukT 72].
Moreover, ^{60}Ni, in comparison with ^{58}Ni, might offer a
unique opportunity to learn something about the isospin
splitting of the E2 (isovector) resonance, as well as the
isospin splitting of the El (isovector) resonance. Isospin
splitting is expected in principle for all isovector states
in nuclei with ground state isospin $T \neq 0$ [FalG 65], but has
neither been quantitatively calculated in theory, nor

reported in the literature for any multipolarity except E1.
From the schematic isospin coupling model [FalG 65], one
would expect a maximum difference in the isovector E2
structure (if it is measurable at all), between nuclei with
$T = 1$ and $T = 2$. The ^{60}Ni nucleus has been well reported
in the literature [BerF 75, YouM 76], but studies made in
this energy range (5 to 40 MeV) using inelastic electron
scattering have beem somewhat unsatisfactory [Gul 69-73].

Foil samples of ^{60}Ni were obtained from Oak Ridge National
Laboratory that were 99.99% ^{60}Ni with impurity traces of
0.01%. Four experiments were done at scattering angles of
60, 75, 90, and 105 degrees. Data were collected with
incident electrons of 102.5 MeV energy. The elastic momentum
transfers squared thus ranged from 0.235 fm^2 to 0.607 fm^2.
Experimental values of the inelastic form factors were
determined from the data, and transition multipolarities
were assigned to the ten observed resonances. Structure at
excitation energies of 7.6, 8.4, 9.9 MeV, which might be
groups of states, are reported here for the first time.
Other resonances of excitation energies 16.5 and 18.5 MeV
already reported in other work were confirmed.

There were several objectives of this research. The
first was to determine the multipolarities of giant
resonances by measuring inelastic electron scattering form
factors, as a function of scattering angle. Second,
inelastic electron scattering could be used to confirm the
existence, as well as energy, strength, and width of dipole

and quadruple giant resonances already observed in photo-
nuclear reactions or inelastic particle scattering. The
third objective was to investigate a range of excitation
energies of ^{60}Ni not previously covered in inelastic
electron scattering experiments.

II. BACKGROUND

Recent investigations of nuclear states in nickel may
be considered to have started with work done at the High
Energy Physics Laboratory at Stanford University during
1960 [CraH 61]. Inelastic scattering of 183 MeV electrons
through angles ranging from 40° to 90° was observed, leading
to excitation of discrete nuclear excited states in ^{58}Ni and
^{60}Ni. The excitation energies were below 8 MeV, and a Born
approximation analysis of the measured inelastic form
factors was used to deduce the multipolarities. The E2
transition to the first excited state of ^{60}Ni was found at
1.33 MeV excitation energy, as were also the E4 transitions
at 2.50 MeV and 5.1 MeV. E4 transitions were also found in
^{58}Ni at 3.5 and 7.55 MeV.

Shortly afterward, in 1962, a study was made of collective
excitations in ^{58}Ni and ^{60}Ni at the Argonne National
Laboratory [Bro 63]. Inelastic scattering of 43 MeV alpha
particles was used to compare the relative strengths of
excited levels in both nickel isotopes. In ^{58}Ni a two-
phonon group corresponding to a known 4+ level was seen at
2.47 MeV; and in ^{60}Ni excitations were identified at the
2.50, 2.16, and 2.29 MeV excitation energies which could be
related to 4+, 2+, and 0+ levels, respectively. Groups
whose angular distributions resembled those of the collective
3- levels were seen at higher excitation energies of 6.8 MeV

in ^{58}Ni and 6.2 MeV in ^{60}Ni. In addition, possible 4+
states were found in ^{58}Ni at 5.5 MeV and ^{60}Ni at 5.1 MeV as
their angular distributions showed a good resemblance to the
distorted wave Born approximation values calculated for a
one-phonon 4+ collective level.

A study was made of the nuclear states of ^{60}Ni at the
Laboratory of Nuclear Science, Tohoku University, in 1968
[TorK 69]. Inelastic scattering of 183 and 205 MeV electron
beams in the Tohoku 300 MeV linear accelerator produced
data which were analyzed using the Born approximation and
the Helm model to determine multipolarities and reduced
transition probabilities. A total of eleven resonances were
found between 1.0 and 7.5 MeV excitation energies. Three in
the range of interest were: 6.20 (3-), 6.85 (2+,5-), and
7.05 (3-) MeV.

In 1968, the giant resonance region in ^{58}Ni and ^{60}Ni
was investigated with electrons of about 200 MeV primary
energy, in the excitation energy region between 10 and 30
MeV [GulA 69]. A giant resonance form factor was obtained
from the data for ^{60}Ni which was found to be in close
agreement with the predictions of the dynamic collective
model [Dre 68]. In addition, the giant resonance form
factors of both nickel isotopes were found to be independent
of atomic weight. This experiment, as we now know, was the
first (e,e') experiment which excited the E2 giant resonance,
but the data were inadequately analyzed, and the existence

14

of the E2 giant resonance was overlooked. After the existence of such a quadrupole mode had been established as a general feature of heavy (A > 40) nuclei, the same data were re-examined [Gul 73]. Resonances at excitation energies of 13.0, 16.3, and 28.5 MeV were observed. Form factors for the 13.0 and 16.3 MeV excitation resonances were calculated and it was found that they corresponded to a quadrupole (E2) resonance, and the well-known giant dipole (E1) resonance, respectively.

Measurements of the analyzing power and the differential cross section in the nuclear continuum for the reaction ^{58}Ni (p,p') from polarized protons of 60 MeV [KocB 73] gave controversial results for the quadrupole giant resonance at a 16.5 MeV excitation energy [Ref. 4 in Ref. (ChaB 75)]. While inelastic deuteron scattering with deuteron energies of 46 and 70 MeV, by the same authors [ChaB 75], demonstrated significant advantages in studying isoscalar giant resonances with deuterons compared to other projectiles. Distorted wave Born approximation predictions suggested that the resonance differential cross section in deuteron inelastic scattering would be sensitive to the transition multi-polarity, particularly in distinguishing between E2 and E0 excitations. Angular distributions calculated using the distorted wave Born approximation were compared with measurements of the 16.5 MeV resonance, and definite indications of its quadrupole character were found.

Also of great assistance in the data reduction and calculations of this experiment was the information from photoneutron cross sections [BerF 75]. Knowledge of specific energies, strengths, and widths of the El resonance(s) provided a starting point in the analysis of the ^{60}Ni spectra in the range from 12 to 25 MeV. In contrast, (α,α') measurements are believed to excite mainly the E2 (isoscalar) resonance. Consequently, the results of Reference [YouM 76] were also used as aids in fitting the spectra.

III. THEORY

A. ELECTRON SCATTERING EXPERIMENTS

The electromagnetic interaction between charge, current, and magnetic moment of a nucleus with the relativistic electron's electromagnetic field is well understood. Quantum electrodynamics and the Dirac equation, describe this interaction. Analysis of electron scattering data provides information about the target nucleus without inter- ference of the imperfectly understood strong interaction. The part of the matrix element containing the strong inter- action of the nuclear forces can be clearly and cleanly separated from the parts involving the electron probe. Heavy particle reactions used for study of nuclear structure are hampered by the intrusion of the nuclear force. The third principal method used in the study of nuclear structure is nuclear absorption and scattering of photons. However, photons cannot reveal ground state information because the momentum transfer q of reactions involving photons is determined by the nuclear excitation, ω. Electron scattering has neither of the disadvantages noted for the other two experimental techniques, and thus is less restrictive. The momentum tranferred by electron scattering can be varied over a wide range because it is expressed by

$$\underset{\sim}{q} = \underset{\sim}{k}_1 - \underset{\sim}{k}_2$$

17

where q is the momentum-energy transfer four vector, and
k_1 and k_2 are the incident and scattered electron momenta
four vectors, respectively. The momentum transfer depends
on the incident and scattered electron energies E_i and E_f,
respectively, and also on the scattering angle θ. q^2 is
given by the expression

$$q^2 = -4E_i E_f \sin^2\left(\frac{\theta}{2}\right)$$

Because q can be varied at a constant nuclear excitation
energy, $E_x = E_i - E_f$, the analysis of scattered electron
momenta can determine nuclear excitations not observed in
photonuclear experiments. Use of heavier charged particles
for nuclear structure investigations enjoys this same
advantage over the photon absorption method. However, heavy
particles are limited in their ability to excite magnetic
transitions and their energies must be restricted to remain
below the Coulomb barrier energy.

The form factor (F^2) is the Fourier transform of the
charge density, for electron scattering, and is only a
function of q^2. To the extent that nuclear wave functions
are known, F^2 can be calculated theoretically. For elastic
electron scattering, in which the nucleus is left in the
ground state, the transition charge density, $\rho(\vec{r})$, depends
on the nuclear wave functions that are solutions of the
wave equation describing the nucleus. Because of the lack
of exact knowledge of nuclear forces, the correct $\rho(\vec{r})$ to

18

be used is approximated by various models. Often, the
starting point for a calculation is just a type of wave
function known to result from a given nuclear model. The
resulting form factor is compared with the experimental
result, because the experimental measurement of the form
factor is one of the primary goals of electron scattering.
In principle, the nuclear form factor yields all the
desired information of the nuclear structure. The term
form factor really only has meaning in the PWBA (Plane Wave
Born Approximation), but the relation

$$|F(q^2)|^2 = \frac{[\frac{d\sigma}{d\Omega}]_{exp}}{[\frac{d\sigma}{d\Omega}]_{Mott}} \quad .$$

is often used for heavy nuclei, where the distorted wave
Born approximation cross sections have to be used, as
defining a "form factor".

For inelastic electron scattering, the nucleus is left
in an excited state that may be either a bound inelastic
or an unbound state. If it is excited to a bound inelastic
state, the nucleus eventually returns to the original ground
state. If it is excited to an unbound state, the nucleus
may be transformed by particle decay. The general form of
the equations defining the form factor, as above, for
inelastic electron scattering is the same as for elastic

electron scattering, but their detailed meanings are different. Inelastic electron scattering form factors are calculated from transition matrix elements in which the initial and final nuclear wave functions are different.

B. DISTORTED WAVE BORN APPROXIMATION (DWBA)

A detailed analysis of the virtual photon which carries the momentum transferred in an (e,e') reaction shows that it can be decomposed into transverse electric and magnetic fields as in a real photon, as well as a longitudinal electric field or Coulomb part that corresponds to the static electric field. The form factors that arise from elastic or inelastic scattering of electrons can in turn be related directly as arising from these different field components. The form factor can consist of the sum of such terms for a given reaction; it can also be given by a single term. If the PWBA were used to derive an expression for the inelastic electron scattering differential cross section, $|\frac{d\sigma}{d\Omega}|_{PWBA}$, it would result in the sum over the separate cross sections of the electric and magnetic multipole transitions. The plane wave Born approximation describes both the incoming and outgoing electrons with the use of plane-wave wave functions. When the nuclear charge, Z, is such that $Z\alpha$ is no longer much less than unity, where α is the fine structure constant ($\alpha \cong 1/137$) the electron wave function is distorted by the strong electric field of

the nucleus and cannot be approximated as a plane wave.
In that case, electron wave function solutions of Dirac's
equation which take into account the ground state charge
distribution are utilized. The PWBA wave solutions are thus
replaced by phase shifted spherical waves. The approximation
is then called the distorted wave Born approximation (DWBA).
Computer computations are required to arrive at solutions
for nuclei of finite spatial extent.

C.   NUCLEAR MODELS

The generalized Goldhaber-Teller model of nuclear
transition charge density as described by Überall [Übe 71],
assumes nuclei are composed of four interpenetrating fluids;
protons with spin either up (↑) or down (↓) and like states
for neutrons. Two of these states oscillating directly out
of phase against two others yield collective vibrational
modes of the nucleus that are evidenced by giant resonances
of particular multipolarity. Goldhaber and Teller [GolT 48]
discussed protons (p↑,p↓) oscillating against neutrons (n↑,n↓).
However, (p↑,n↑) oscillating against (p↓,n↓) and (p↑,n↓)
against (p↓,n↑) are also possibilities. All four fluids
oscillating in phase against each other would produce a
compressional model called a monopole vibration. Goldhaber
and Teller assumed the ground state charge density $\rho_o(r)$
was rigidly displaced and the total charge density could
be expressed

$$\rho(r) = \rho_o(r) - \frac{1}{2}\vec{d} \cdot \nabla \rho_o(r)$$

21

where $\vec{d}$ is the small displacement between the neutron and proton mass centers. The expression above describes dipole motion, but Überall [Übe 71] demonstrated that it could be generalized to include other multipole vibrations if the ground state charge density were deformed by a scale factor η. The total charge density is then assumed to be $\rho(r) = \rho_o(r) + \rho_{tr}(r)$ with the transition charge density,

$$\rho_{tr}(r) = -\eta r \left[\frac{d\rho_o(r)}{dr}\right]$$

The transition charge density can be understood as that part of the nuclear matter, in a given nucleus, that takes part in the interaction. For example, single particle transitions would only affect those nucleons on or near the surface of the nucleus; so that the term ρ_{tr} would have an appreciable amplitude only at a radius in the region of the surface. The rest of the nucleus would remain undisturbed, i.e., $\rho(r) = \rho_o(r)$, for single particle transitions. The scale factor η can be expanded as a multipole series:

$$\eta = \sum_{\ell m} \alpha_{\ell m} \left(\frac{r}{R}\right)^{\ell+k_\ell-2} Y_{\ell m}(\theta, \phi)$$

where k_ℓ is twice the Kronecker delta, and R is a reference radius used to make η dimensionless. Similar multipole expansions are used to describe the current and magnetization densities.

Steinwedel and Jensen [SteJ 50] proposed a model which relied on a rigid nuclear surface and assumed that the

22

collective vibrations of neutrons and protons were described
as changes in the two fluids' relative densities. Überall
[Übe 71] notes that this model requires the charge density
to be constant,

$$\rho(r) = \rho_p(r) + \rho_n(r) = \text{constant}$$

for $r = R_o$ ($R_o = 1.2 \ A^{1/3}$, where A is the atomic weight).
A scale factor is also used with the Steinwedel and Jensen
model to describe general vibrational modes, such that:

$$\rho_p(\vec{r},t) = \frac{Z}{A} \rho_o + \eta(\vec{r},t)$$

and

$$\rho_n(\vec{r},t) = \frac{N}{A} \rho_o - \eta(\vec{r},t)$$

With a rigid nuclear surface, there can be no charge density
flux through the surface, and:

$$[\frac{\partial \eta}{\partial r}]_{r=R_o} = 0$$

where η is again delineated by a multipole expansion.

Ziegler [Zie 67] related the reduced transition probabil-
ities (B-values) for transverse electric and magnetic
transitions to the form factors with the equation:

$$|F(q^2)|^2 = \frac{4\pi}{z^2} \left(\frac{\lambda+1}{\lambda}\right) \left[\frac{q^\lambda}{(2\lambda+1)!!}\right]^2 B\left(\begin{smallmatrix}E\\M\end{smallmatrix}\lambda,q\right)$$

where λ indicates the number of units of angular momentum transferred to the nucleus in the reaction. The theoretical form factor due to the Coulomb, or longitudinal, part of the interaction is written

$$|F(q^2)|^2 = \frac{4\pi}{z^2} \{q^{2\lambda}/[(2\lambda+1)!!]^2\} \cdot B(C\lambda,q)$$

The coefficients of these equations, $B\left(\begin{smallmatrix}E\\M\end{smallmatrix}\lambda,q\right)$, are the reduced nuclear transition probabilities. Adler, et al. [AdlB 56], defines reduced transition probabilities by the expression

$$B(\lambda,q,J_i \rightarrow J_f) = \frac{1}{2J_i+1} |<J_f||M(\lambda,q)||J_i>|^2$$

where $M(\lambda,q)$ is the particular transition operator, and J_i and J_f are respectively the initial and final angular momenta of the target nucleus. The B-values measured in electron scattering are functions of q, and are equal to the B-values obtained in photoneutron work in the limit of $q \rightarrow k$, the proton energy required to excite the transition. That is,

$$B(\lambda,q,J_i \rightarrow J_f)(e,e') \underset{\lim q\rightarrow k}{=} B(\lambda,J_i\rightarrow J_f)(\gamma,n)$$

Also, within the error of this experiment,

$$B(E\lambda,q=0) \approx B(E\lambda,q=k)$$

is assumed to be correct. The transition operators $\hat{M}(\lambda,q)$ were developed by Ziegler [Zie 67] using the PWBA. For longitudinal (Coulomb) interactions

$$\hat{M}(c\lambda,q) = \frac{(2\lambda+1)!!}{q^\lambda} \int \hat{\rho}_{tr}\ j_\lambda(qr)\ Y_{\ell m}(\theta,\phi)\ d\tau$$

for the transverse electric interaction (current only)

$$\hat{M}(E\lambda,q) = \frac{1}{c}\frac{(2\lambda+1)!!}{q^{\lambda+1}(\lambda+1)} \int \hat{j}_N \cdot \overline{\nabla}\times L\ [j_\lambda(qr)\ Y_{\ell m}(\theta,\phi)]\ d\tau$$

and for the transverse magnetic interaction (current only)

$$\hat{M}(M\lambda,q) = -\frac{i}{c}\frac{(2\lambda+1)!!}{q^\lambda(\lambda+1)} \int \hat{j}_N \cdot \hat{L}\ [j_\lambda(qr)\ Y_{\ell m}(\theta,\phi)]\ d\tau$$

In the equations above:

$\hat{\rho}_{tr}$ = transition charge density operator

$j\lambda(qr)$ = spherical Bessel function of order λ

$\hat{j}_N$ = nuclear current operator

$\hat{L}$ = orbital angular momentum operator.

Model dependent inelastic form factors were calculated using the distorted wave Born approximation (DWBA) with the computer code GBROW [Zie 67]. For heavy nuclei, reduced nuclear transition probabilities (the B-values) can only be extracted from data with model dependent calculations. The model used was the generalized Goldhaber-Teller model

25

described by Überall [Übe 71]. The DWBA form factor, normalized to $B(E\lambda) = 1$ fm^2, is compared with the experimental form factor, $[F]^2_{exp}$ over a range of momentum transfer. The ratio yields an experimental value of the reduced nuclear transition probability, B_{exp}. As a check that observed resonances are indeed collective phenomena, a comparison of experimental with single-particle reduced transition probabilities is made. The ratio should be significantly greater than unity for giant multipole resonances because the ρ_{tr} term for single-particle reactions only involves nucleons on the nuclear surface, while nucleons throughout the nucleus are involved in the ρ_{tr} term for giant resonances. Giant resonances should also deplete an appreciable amount of the appropriate energy weighted sum rule for the same reason. An observed resonance should not considerably exceed the iso-scalar sum rule for the assumed transition. In Weisskopf units [SkoH 66], the single-particle reduced transition strengths are

$$B(E\lambda)_{spu} = \frac{e^2(2\lambda+1)}{4\pi} \left(\frac{3}{\lambda+3} R^\lambda\right)^2 fm^{2\lambda}$$

and

$$B(M\lambda)_{spu} = \frac{10e^2(2\lambda+1)}{\pi} \left(\frac{3}{\lambda+3}\right)^2 R^{2\lambda-2} fm^{2\lambda-2}$$

where $R_o = 1.2 \ A^{1/3} = 4.70$ fm for ^{60}Ni. Evaluation of the $E\lambda$ transition strength is also made by expressing it as a

26

fraction of the appropriate energy-weighted sum rule (EWSR).
The isoscalar ($\Delta T=0$) excitation mode sum rule given by
Nathan and Nilsson [NatN 66] for $L > 1$ is,

$$S(E\lambda, \Delta T=0) = \sum_{f} (E_f - E_i) \, B(E\lambda, q)$$

$$= \frac{Z^2 e^2 \lambda (2\lambda+1)^2 \hbar^2}{8\pi A M_p} \, \langle R^{2\lambda-2} \rangle$$

where M_p is the proton mass. The sum rule for $L > 1$ for
isovector transitions ($\Delta T=1$) is related to the isoscalar
sum rule by

$$S(E\lambda, \Delta T=1) = S(E\lambda, \Delta T=0) \, \left[\frac{N}{Z}\right]$$

where N is the number of neutrons. Ferrell [Fer 57] writes
the corresponding isoscalar monopole (E0) excitation sum
rule as

$$S(E0) = \sum_{f} (E_f - E_i) \, |M_{fi}|^2$$

which becomes

$$S(E0) = \frac{\hbar^2 Z}{M_p} \, \langle R^2 \rangle$$

where M_{fi} is the monopole transition matrix element.
Warburton and Wensser [WarW 69] express the (E1) resonance
sum rule

27

$$S(E1) = \frac{9e^2 \hbar^2}{8\pi M_p} \left(\frac{NZ}{A}\right)$$

Throughout this thesis the $\langle R^{2\lambda} \rangle$ needed for the sum rules were calculated by numerical integration of the ground state charge distribution. The values c = 3.84 fm and t = 2.50 fm [deJd 74] were used.

D. GIANT RESONANCE PHENOMENA

The term giant resonance was first used to describe what is known to be the giant electric dipole resonance (GDR). Goldhaber and Teller's paper proposing these features as resonance structures also implied that different giant resonance multipolarities might exist [GolT 48]. Goldhaber and Teller first attempted to explain the giant dipole resonance based on their collective model which assumed neutrons and protons to behave as two interpenetrating incompressible fluids (see, however Migdals paper [Mig 44], who proposed this model four years before Goldhaber and Teller). This classical approach considered the two fluids to be displaced relative to each other during dipole oscillations, such that they did not overlap near the nuclear surface. The restoring force was assumed proportional to surface area, or R^2, and the resultant harmonic motion exhibited a frequency proportional to the square root of the force divided by the mass,

$$\omega \sim \left(\frac{R^2}{R^3}\right)^{1/2} = R^{-1/2}$$

Because $R \sim A^{1/3}$ the harmonic oscillator energy should be proportional to the negative one-sixth root of A: $E(GDR) \sim A^{-1/6}$. Goldhaber and Teller [GolT 48] found the relation to be approximately:

$$E(GDR) \cong 40A^{-1/6}$$

Their model did not allow for the possibility of a monopole resonance, since the assumption of incompressible fluids restricts relative charge density changes. However Überall's generalization of this model does admit of monopole transitions in the expansion of the scale factor η. The Steinwedel and Jensen model [SteJ 50] assumed collective motion within a rigid boundary, and the energy of the GDR for spherical nuclei is given by

$$E(GDR) = \frac{2.08}{R} \left(\frac{8KNZ}{M*A^2} \right)^{1/2}$$

where M* is the nucleon effective mass, and K is the symmetry energy from the semi-empirical mass formula. The nuclear radius is proportional to $A^{1/3}$, so that $E(GDR) \sim A^{-1/3}$. Hayward [Hay 69] found that $E(GDR) = 80 \, A^{-1/3}$ MeV.

IV. DATA ACQUISITION

A self-supporting foil of ^{60}Ni with a mass density of 135 mg/cm^2 was obtained from Oak Ridge National Laboratory and placed in the scattering chamber of the NPS LINAC, and positioned for transmission geometry at an angle equal to one-half the scattering angle. The electron linear accelerator facility at the Naval Postgraduate School has been described by Warshawsky and Webber [WarW 73].

Considerable effort and accelerator running time were spent to understand the origin of background radiation. Such background existed without any target, and was detrimental to the quality of the data because it was not always a constant contribution. It varied both with accelerator adjustments and beam intensity. Shielding was re-stacked and added inside the beam deflection system. A major improvement was achieved by shielding the part of the beam pipe in the target room. Lead collimators or plugs with appropriately sized openings were placed before and after the energy defining slits. With the beam deflection magnets, the use of only quadrupole doublet Q3 and Q4 also helped reduce the background. Doublet Q1 and Q2 caused electron orbits which scraped the accelerator beam pipe walls.

In addition, the ten-channel scintillation counter ladder was rebuilt. All plastic scintillator material and most of the phototubes were replaced. The two long backing counters

were modified with phototubes at both ends, rather than at only one end. The signals from the phototubes at the ends of the backing counters were summed. As a result, the pulse output response of those two counters was almost independent of the entry position of the electrons along their lengths. As a result the phototubes could be adjusted to a plateau of lower voltage so that small background pulses were not detectable.

Plateau curves for the entire counting system were measured, and delay curves were optimized. High stability and reproducibility are required for giant resonance measurements, because the resonances themselves are generally small contributions ($\leq 10\%$) to the scattered electron spectrum, the main cross-section arising from radiative processes.

The absolute energy calibration assigned to the energy scale on the data curves was determined by measuring the 15.1 MeV level of ^{12}C.

The magnetic fields in both the accelerator deflection system and the spectrometer were saturated before the runs in order to ensure the correctness of the energy scale and experimental reproducibility. Repeated elastic peaks were reproducible to within one-half of one channel width on the energy scale when the magnets were saturated prior to data collection.

Four experimental runs were conducted at an incident electron energy of 102 MeV and scattering angles of 60, 75,

90, and 105 degrees. All runs measured excitation energies
to 40 MeV. In addition, the inelastic spectrum of the 75
degree run was observed twice with the same accelerator param-
eters to determine if there were significant differences in
the spectra due to machine fluctuations during the course of
the 48 to 60 hour data collection period. These experiments
showed reproducible results, confirming the stability of
experimental conditions. The count rates were maintained
below 50 counts per second per channel to avoid losses due
to electronic dead time in the ladder counter system. The
total charge delivered by the beam was adjusted for each
experiment to maintain approximately a one-percent statistical
uncertainty in the counts per channel. Table I lists the
experimental conditions used for each run.

V. <u>DATA REDUCTION</u>

Data collected by the LINAC ladder counting system were
transferred to a teletype ASR 39 which produced a typewritten
copy as well as a punched paper tape. The NPS Computer
Science Group PDP11-50 Duplex System was used to bring data
from the teletype paper tape to a magnetic tape compatible
with the NPS IBM 360/67 CP/CMS on-line system. The IBM
360/67 on-line system was used to edit and correct the raw
data before it was reduced for use by a fitting program.
This initial data reduction is accomplished by a FORTRAN
computer program which sums the data in each individual
counter of the ladder counting system in the corresponding
bin of excitation energy. The data are normalized to the
same amount of integrated beam. The computer code
consists of six functional parts:

1. Data Intake

This part transfers the measured spectra data into the
computer along with the input parameters necessary to con-
trol the calculations, for example, calculation of the
radiation tail.

2. Elastic Fit

This section fits the elastic peak, which serves as
a normalization cross section for the radiation tail and
inelastic calculations, and as a reference for the excitation
energy. The lineshape of the elastic fit is assumed to con-
sist of two gaussian bell curves; one for the <u>left</u> (low energy)

side, and one with the same height but of independent width for the <u>right</u> (high energy) side. The radiation tail is assumed to have the form of a hyperbola.

3. Radiation Tail

This part calculates points for the radiation tail. The radiation tail is the main portion of the function which describes the total background during the inelastic fit.

4. Inelastic Fit

This is the most essential part of the program because it calculates the desired end product; namely, the reduced matrix elements of the resonance transitions.

5. Numerical Results

This section provides output calculations of the elastic fit parameters, radiation tail calculation results, and the parameters of the inelastic fit. Reduced transition probabilities (B-values) are also shown, either in percentage of sum rule exhaustion or units of $fm^{2\lambda}$, as desired.

6. Plot

This section produces a computer printer plot which exhibits original data points (after background subtraction), the fitted curve (after background subtraction), the single resonance curves, subtracted background, and statistical deviations of the fitted curve from measured data points.

VI. DATA ANALYSIS

Calcomp plots of added single counters with radiation
tail included were produced for each data run. A rough
radiation rail subtraction was drawn in by hand and the
excitation energies of the major structures approximately
located by eye. These resonances were then compared with
transitions reported in [Übe 71], [BerF 75], [FulA 74],
[GulA 69]. Where obvious matches occurred, reported widths
were used. Where no resonance was reported, a starting width
was estimated.

Line shape cards were prepared for the fit program which
included the shape to be used (e.g., Breit Wigner), the
excitation energy, and the full width at half maximum of
the resonance. Excitation energy, width and peak height
are parameters that may be selectively held constant or
freed in achieving a best fit. On the first fitting, energies
and widths were held fixed, and peak heights allowed to
adjust for a best fit. The plot section output was then
examined, the fitted peak heights were recycled as starting
values for the next fitting and other parameters freed. This
iterative technique was repeated, and line shapes were added
and shifted with each fitting in an attempt to improve the
χ^2 per degree of freedom, henceforth referred to as χ^2.
Steady, consistent improvement in the fit was best achieved
by working with the data from several angles simultaneously.

One set of line shape cards was used for all angles, and changes in line shapes were made only when χ^2 improved overall for all angles considered together.

Examination of the spectra with the radiation tail subtracted showed much structure in the range 5 MeV to 13.5 MeV, whereas in the giant resonance region in the range 13.5 MeV to 25 MeV, the striking feature was a large, broad, and relatively smooth cross section, which was much more difficult to break down into its component resonances. Each spectrum was analyzed piecemeal. A good fit was first achieved in the lower energy bound states region and held constant while resonance subtraction techniques were utilized in the giant resonance region.

E1 resonances in ^{60}Ni have been reported, [BerF 75] at 16.3 and 18.5 MeV from (γ,n) experiments. From the reported cross sections, the B values and form factors were calculated. Energies and full widths at half maxima (FWHM) were also taken from the literature. In order to help untangle the multiple contributions to the spectrum, the (γ,n) results for E1 were used as inputs to the fitting process. A given value of the form factor was related to the Fit Program through the peak height. E1 resonances were inserted with Lorentz line shapes with FWHM equal to 2.44 and 6.37 MeV for the resonances at 16.3 and 18.5 MeV, respectively. The formula

$$\int \sigma_\gamma dE_\gamma = \pi^2 \hbar c \alpha \, \frac{8\pi(\lambda+1)k^{2\lambda-1}}{[(2\lambda+1)!!]^2} \, B(\lambda,k) \, , \qquad \text{[IsaB 63]}$$

was used to calculate the cross sections of the E1 in (e,e').

Examination of subsequent Fit Program printouts revealed

positions and approximate widths of other resonances needed

to fit the data. After several iterations, uniformly good

χ^2 values were obtained and tentative assignments of multi-

polarities were made.

DWBA "form factors" as defined above were calculated

with the standard DWBA program [TuaW 68], [Zie 67]. The

Goldhaber-Teller model was used for the electric and magnetic

transitions. These DWBA calculations of F^2 as a function of

q, were produced for the following multipolarities: E0,

E1, E2, E3, E4, M1 non-spin flip and M2 non-spin flip.

The code of Tuan et. al. does not allow the calculation of

magnetic spin-flip transitions. For this purpose the program

of Drechsel [Dre 68] was used. As transition radii for the

M1 spin-flip transition, R_{tr} values of 4.2 fm and 4.7 fm

were used. Plots for each transition were hand-drawn on

three decade, semi-log graph paper. Values of q and F^2_{EXPT}

were obtained for each fitted resonance from the output and

plotted on three decade semi-log overlays with estimated

errors of ± 20%. The overlays were tried in turn on the

DWBA plots of F^2_{DWBA} vs q until the best match of overlay

plot and DWBA curve was achieved, thus tentatively identifying

the resonance.

Although an E2 resonance in ^{60}Ni had been reported

[YouM 76], at 16.5 MeV from (α,α') experiments, initial

results of fitting the data with the previously cited E1
resonances indicated an E3 resonance at 16.5 MeV vice an
E2 resonance. Accordingly, the reported E2 resonance at
16.5 MeV with FWHM of 4.3 MeV was used as an input to the
fitting process in a fashion identical to that used for the
insertion of the E1 resonance. Although relatively good
χ^2 values were obtained, results of this fitting were incon-
clusive because no other resonances were positively identified.

Next, a superimposed DWBA theoretical plot of F^2 vs q
for E1, E2, E3, and E4 resonances was prepared (Figure 6).
Utilizing this multiple plot, it was seen that an E2 reson-
ance would remain almost constant with the change in angle
from 60° to 105°, whereas an E3 or E4 would grow with in-
creasing angle and an E1 would shrink with increasing angle.
The data envelope in the giant resonance region was studied
and the observation made that the data remained relatively
constant in the center, increased in size on the left flank,
and subsided on the right flank, with increasing angle,
indicating a possible E3 or E4, E2, and E1 from left to right,
respectively, in the giant resonance region. It was also
noted from examination of Figure 6 that subtraction of too
large an E1 resonance could cause the remaining data to be
fitted by an E3 resonance where, in fact, an E2 might reside.

Consequently, the E1 insertion technique was again
attempted, this time reducing the B-value of the reported
E1 resonance at 16.3 MeV by 1/2 for all four angles, inserting
a line shape at 16.5 MeV with a FWHM of 4.3, and freeing all

heights except the two E1 resonances at 16.3 and 18.5 MeV.
The resultant DWBA plot of the resonance at 16.5 MeV was
estimated to look slightly more like an E2 than an E3.
Finally, the E1 resonance reported at 16.3 MeV was eliminated
entirely and a fit made fixing only the heights of the E1
resonance reported at 18.5 MeV. χ^2 values of .71, .82,
1.0, and 1.1 were achieved for the angles of 60°, 75°, 90°,
and 105°, respectively. Resonance plots with tentative
assignments of multipolarities for this fitting are shown
as Figures 7 through 18. Next, all nine line shapes except
the E1 at 18.5 MeV were freed in energy. Fit input cards
were updated and the energies and widths and heights freed
for the same nine line shapes. χ^2 improved to values of
.64, .76, .87 and .87 for 60°, 75°, 90°, and 105° respectively.
Again, tentative identification of the resonances was made
by DWBA plot, Figures 7 through 18.

From both sets of fits, reduced transition probabilities
and energy weighted sum rule percentages were calculated.
These results are presented in Tables II, III, and IV.
Weisskopf single particle units and energy weighted sum
rules are presented in Table V.

VII.   ERROR ANALYSIS

In the type of analysis performed there is one inherent difficulty in the error analysis: the statistical and systematic errors from the measurement alone (errors produced by count rate, accuracy of the beam monitor, etc.) are obviously much smaller than the variance of the extracted form factor. Nonetheless the statistical error for the form factor (equal area) extracted from one measurement at one angle has some bearing on the weight this measurement should carry.   In principle the error of the area, A would be calculated with

$$\Delta A = \sqrt{\Delta \Gamma^2 + \Delta ht^2}$$

(Γ = width, ht = peak height).   However, in the "limited freedom" analysis Γ was held fixed.   Still, the statistical error of the area from the height alone will reflect the relative weight of the measurement.   Consequently, the averaged reduced transition probability, $\overline{B}$, was calculated by using this error.   The relation for a weighted arithmetic mean is

$$\overline{B} = \frac{\sum\limits_{i=1}^{n} W_i B_i}{\sum\limits_{i=1}^{n} W_i}$$

where

$$W_i = \frac{1}{\sigma^2} .$$

Weighted average B values are calculated for the
"limited freedom" runs only, and are included in Table III.
The error in $\bar{B}$,

$$\Delta B = \frac{\bar{B}}{\sum\limits_{i=1}^{n} W_i} .$$

For the "best χ^2" analysis an unweighted average was
taken and standard deviation from the mean reported as the
error.

Percent error of F^2 for each DWBA plot is given in
Table II.

VIII. DISCUSSION

A. COLLECTIVE RESULTS

The data analysis shows the existence of ten states at excitation energies of 6.15, 7.02, 7.59, 8.43, 9.93, 11.78, 12.91, 15.0, 16.5, and 18.5 MeV in the inelastic electron spectrum of ^{60}Ni. In the original data which extends to 50 MeV excitation energy, another resonance was found at 31.9 MeV excitation energy, but was not thoroughly investigated. In addition, two other states were indicated by the data; one at 16.3 MeV excitation energy in the 60 degree data, and another at 9.5 MeV excitation energy in the 60 degree and, to a lesser extent, in the 75 degree data. The latter two are discussed further in the detailed presentations of the states found at 16.5 and 9.93 MeV excitation energy, respectively.

Two distinctly different philosophical approaches were used in the analysis of the data. On the one hand, limited or selective freedom of the two parameters excitation energy and strength was employed, while the full width at half-maximum (FWHM) was varied by trial and error to minimize the χ^2 fit. Alternatively, for comparison, the FWHM and heights were permitted to vary freely for the best fit in the Fit program, and the best χ^2 fit obtained. The results of these two methods are compared in the discussions of individual resonances.

In the following summaries, unique assignments were not always possible. For those cases, additional data covering a broader range of momentum transfer would be needed.

B.   RESONANCES AND CHARACTERISTICS

    1.   <u>6.15 MeV</u>

        An E3 transition was reported by Torizuka in 1969 [Tork 69] at 6.20 MeV excitation energy. The existence of a resonance in this region is clearly seen in Figures 2, 3 and 4. Identification by DWBA form factor plot, Figure 7, slightly favors E3 over E2. This resonance exhausts 11.7% of the energy weighted sum rule for E3, utilizing the limited freedom analysis, henceforth referred to as the "(a)" result; and 9% utilizing the best χ^2, or "(b)" result. The Torizuka experiments in 1969 utilized a maximum energy of 250 MeV. The .05 MeV difference in reported excitation energies is within the errors of our calibration. In any case, .05 MeV represents approximately 10% of the average resolution for these experiments in ^{60}Ni. B-values are: (a) 27 and (b) 21 Weisskopf units.

    2.   <u>7.02 MeV</u>

        Torizuka in 1969 reported an E3 transition at 7.05 MeV. This resonance is clearly seen as a sharp peak in the experimental data, Figures 2, 3 and 4. Identification by DWBA form factor plot, Figure 8 is E3, at an excitation energy of 7.02 MeV, agreeing closely with the value of 7.05 MeV reported by Torizuka. The "best χ^2" value of excitation

energy is reported for this resonance because of the highly structured nature of the data in this region, which provides semi-isolation of this resonance from its neighbors on either side. Hence, freeing FWHM for best fit by Fit program does not result in unwanted influence by neighboring resonances. This transition exhausts (a) 11.7 (b) 10.4% of the EWSR. B-value is 21 Weisskopf units. Another possible identification of this and all other reported E3 transitions is as an M2 transition. Examination of the DWBA form factor plot shows that in the momentum transfer region of interest, a case may also be made for identification as an M2, although the fit is not quite as good as for the E3 curve.

3. 7.59 MeV

Unreported in the literature, this transition plots slightly better as an E3 than an E2, Figure 9. As an E3, it exhausts (a) 7.2 (b) 6.2% of the EWSR. As an E2 (2) 5.2 (b) 4.8% of the EWSR would be exhausted. B-values are: E3, (a) 13.2 (b) 11.6 SPU and E2 (a) 3.9 (b) 3.6 SPU.

4. 8.43 MeV

Identified as an E2 in both DWBA form factor plots, Figure 10, this resonance is previously unreported in the literature. Percentage of EWSR exhausted is (a) 12.6 (b) 14.3. B-value is (a) 8.5 (b) 9.7 SPU.

5. 9.93 MeV

This transition, not previously reported, was seen most strongly in the 60° and 75° data, subsiding quickly at the larger angles. It is identified as an E1 on DWBA form

factor plot, Figure 11; whereas, it is not identifiable at all in the "best χ^2" DWBA form factor plot, same figure. This may be explained by first noting the lack of structure in the data envelope in the region 8.5 to 10.5 MeV at the larger angles, 90° and 105°. In the limited or selective freedom mode, this resonance was first seen at 75° where the data has some structure, fitted at that angle and then held constant in excitation energy and FWHM for 90° and 105° where its contribution was much smaller, allowing only the peak height to be fitted. However, in the best χ^2 mode, the lack of structure at the larger angles allowed the line shape to wander significantly from angle to angle, losing its identity in the process. What caused the line shape to wander? Examination of the complete spectrum from the sub-sequently obtained 60° run showed a probable resonance at about 9.5 MeV excitation energy. Comparison with the 75° data confirmed the likelihood of a resonance at that energy, however the resonance is weaker at 75° than at 60°, and not at all noticeable at 90° or 105°. This probable, unfitted resonance at 9.5 MeV behaves like another very small E1. The fact that it was an unfilled area in the data in the neighborhood of an identified E1 perhaps caused the E1 at 9.9 MeV to wander when given full freedom in the best χ^2 mode. The probable resonance at 9.5 MeV was not investigated further. The E1 resonance at 9.9 MeV exhausts 2.2% of the EWSR with B-value 0.35 SPU. The resonance at 9.5 MeV, if it exists, would most likely be even smaller.

6. __11.8 MeV__

This is another small, unreported resonance identi-
fied as either: (a) E2, 3.0% of EWSR, 1.5 SPU or (b) E4,
28 % of EWSR, 43 SPU, Figures 12, 13. As the large, smooth,
relatively featureless giant resonance region is approached,
it becomes more dangerous to allow the FWHM freedom of fit.
With so many component resonances in close contact, a small
change in FWHM of one large resonance can mean a large
change in cross section of a smaller one. One must be
increasingly selective in allowing fit program freedom to
achieve best fit in the giant resonance region.

7. __12.9 MeV__

This resonance reported [Gul 74] as an E2 at 13.0
MeV is identified as (a) E3, 8.5% of EWSR, B = 9.3 SPR or
(b) E3, 9.0% of EWSR, B = 9.9 SPU. See Figure 14.

8. __15.0 MeV__

This is the last previously unreported resonance
identified in these experiments. Observed to be (a) E4,
18.6% of EWSR, with B = 34 SPU or (b) E4, 28.4% of EWSR,
with B = 54 SPU, Figure 15. In this case, when the FWHM
was given freedom in the best χ^2 fitting, the width increased
from 1.76 to 2.24 ± .51 , a 28% increase in the width with
a variation of 23 % of the new value. Clearly, this kind
of large change of width with angle is not a physical result,
but is rather a typical result of a line shape fitting pro-
gram working to achieve the best χ^2. Further, it is an
indication that perhaps not all resonances have yet been

46

found, or that their parameters are not yet close enough to correct values to ensure a good fit with minimal iterations.

9. <u>16.5 MeV</u>

This resonance has been reported as an E2 from (α,α') work [YouM 76] but as an El at 16.3 MeV from (e,e') experiments [Gula 73]. So confusion has existed concerning this region. A line shape was inserted at 16.5 MeV with FWHM of 4.3 reported from (α,α') experiments and height freed for best fit. The neighboring resonance at 18.5 MeV was inserted and held constant as previously described. This limited freedom approach produced an E2 identification (Figure 16), 61% of the EWSR was exhausted, B = 21 SPU, a collective mode indicative of a giant resonance. When the best χ^2 approach was utilized, an E3 identification resulted (Figure 17), with 153% of the EWSR exhausted and B = 131.9 SPU. Sum of all E3 % EWSR exhausted would be approximately 180% utilizing the best χ^2 identification for this resonance, whereas the sum of all E2 resonances is approximately 82% EWSR utilizing the limited freedom identification of E2 for the resonance. Considering the percentage of EWSR exhausted, fitting techniques utilized and the findings reported in (α,α') at Texas A&M, the E2 identification is the preferred one.

Initially, the El resonance observed in (γ,n) [BerF 75] was inserted at 16.3 MeV at the reported strength, then cut in half, then eliminated as it seemed the data would not

47

support both the E2 at 16.5 and the El at 16.3 MeV. However, in the final data run for 60° (Figure 5), there appears a small amount of unfitted cross-section at 16.3 MeV which does not appear in the larger angles. An El resonance would behave in exactly this fashion, especially a small one. It appears that there may indeed be a small El at 16.3 MeV excitation energy which the data at 60° would support, but which does not manifest itself at any other, larger angle. This agrees with the literature. The Soviets, measuring at scattering angles from 20 to 70 degrees in 10 degree steps, observed this as a strong resonance which becomes weak in just the region where our measurements overlap; namely, 60 degrees.

10. <u>18.5 MeV</u>.

This El resonance has been reported observed in (γ,n) experiments [BerM 75]. The parameters arising from the fitting of a Lorentz shape to that data were utilized to insert the shape, and the shape held constant for all fitting processes. Of course, this resonance plots as an El. This method, herein referred to as resonance substraction, was utilized as a means of untangling the component resonances of the giant resonance region.

IX. CONCLUSIONS

Giant multipole resonance studies by inelastic electron scattering in ^{60}Ni show at least ten identified structures in the excitation range of 6 MeV to 30 MeV. These "resonances" occur at excitation energies of 6.15, 7.02, 7.59, 8.43, 9.93, 11.8, 12.9, 15.0, 16.5, and 18.5 MeV. The 6.15 and 7.02 MeV resonances have been reported in the electron scattering work and are known as E3. The five resonances indicated at 7.59, 8.43, 9.93, 11.8, and 15.0 MeV are reported for the first time. The E3 resonance at 12.9 has been previously reported in Soviet work as an E2 at 13.0 MeV. The resonance at 16.5 MeV has been reported in (α,α') and (e,e') work and is known as electric quadrupole. The 18.5 MeV resonance is known from (γ,n) work as an electric dipole resonance.

With these experiments, an exploration gap has been filled. The excitation range from 7.5 MeV to 10 MeV has been reported for the first time. Also, several of the newly reported resonances are above the neutron threshold and in the lower portion of the giant resonance region, at 11.8, 12.9, 15.0 MeV.

TABLE I. EXPERIMENTAL CONDITIONS
INELASTIC ELECTRON SCATTERING FROM ^{60}Ni

Experimental Scattering Angle (Degrees)	Measured Incident Energy (MeV)	Elastic Peak Resolution (MeV)	Momentum Transfer Squared $q^2(fm^2)$
60	102.01	0.473	0.235
75	102.10	0.517	0.359
90.9	102.10	0.507	0.482
105	102.10	0.516	0.607

*Target thickness 135 mg/cm^2 for all runs.

TABLE II   INELASTIC FORM FACTORS SQUARED
INELASTIC ELECTRON SCATTERING FROM ^{60}Ni

INELASTIC SCATTERING ANGLE

Excitation Energy (MeV)	60 DEG	ERROR %	75 DEG	ERROR %	90 DEG	ERROR %	105 DEG	ERROR %
6.14 ± .037	-	-	3.87×10^{-4}	5.03	5.90×10^{-4}	3.37	4.58×10^{-4}	5.47
7.01 ± .040	-	-	3.32×10^{-4}	4.27	4.71×10^{-4}	2.97	4.54×10^{-4}	4.03
7.59 ± .022	-	-	1.96×10^{-4}	5.66	2.27×10^{-4}	4.34	2.29×10^{-4}	5.41
8.43 ± .002	-	-	6.01×10^{-4}	4.47	4.88×10^{-4}	5.05	3.89×10^{-4}	7.99
9.93 ± .053	-	-	7.77×10^{-5}	13.9	2.64×10^{-5}	35.3	1.14×10^{-5}	102
11.8 ± .000*	-	-	9.14×10^{-5}	15.9	8.98×10^{-5}	14.7	7.43×10^{-5}	22.2
12.9 ± .000*	-	-	1.18×10^{-4}	10.7	1.78×10^{-4}	6.53	1.78×10^{-4}	8.21
15.0 ± .000*	5.67×10^{-5}	38.0	5.18×10^{-5}	31.6	1.18×10^{-4}	13.3	1.86×10^{-4}	10.9
16.5 ± .000*	8.8×10^{-4}	6.05	1.21×10^{-3}	3.55	1.51×10^{-3}	2.76	1.16×10^{-3}	4.67
18.5 ± .000*	1.17×10^{-3}	0.00	9.94×10^{-4}	0.00	5.83×10^{-4}	0.00	2.99×10^{-4}	0.00

* Energies were fixed

TABLE III REDUCED TRANSITION PROBABILITIES AND SUM RULES
(LIMITED FREEDOM ANALYSIS)

E_x (MeV)	λ	Γ (MeV)	$\bar{B}_{calc}$ $fm^{2\lambda}$	Error, $\bar{B}$	Strength in SPU	% EWSR Dissipated
6.14 ± .04	E3	0.58	1.55×10^4	2.0×10^2	27.0	11.7
7.01 ± .04	E3	0.58	1.37×10^4	1.35×10^3	23.8	11.7
7.59 ± .02	E2*	0.58	9.72×10^1	2.10×10^1	3.9	5.2
	E3	0.58	7.79×10^3	1.11×10^3	13.5	7.2
8.43 ± .00	E2	1.59	2.13×10^2	2.38×10^1	8.4	12.6
9.93 ± .05	E1	0.58	4.87×10^{-1}	1.80×10^{-1}	.35	2.2
11.8	E2	1.2	3.66×10^1	3.48×10^{-1}	1.45	3.0
12.9	E3	1.2	5.36×10^3	4.89×10^2	9.3	8.5
15.0	E4	1.76	5.87×10^5	5.68×10^4	34.9	18.6
16.5	E2	4.3	5.29×10^2	5.37×10^1	21.0	61.1
18.5	E1	6.37	7.58	4.45×10^{-1}	5.5	63.7

*Based on DWBA plots, all E2 resonances could be E0, and all
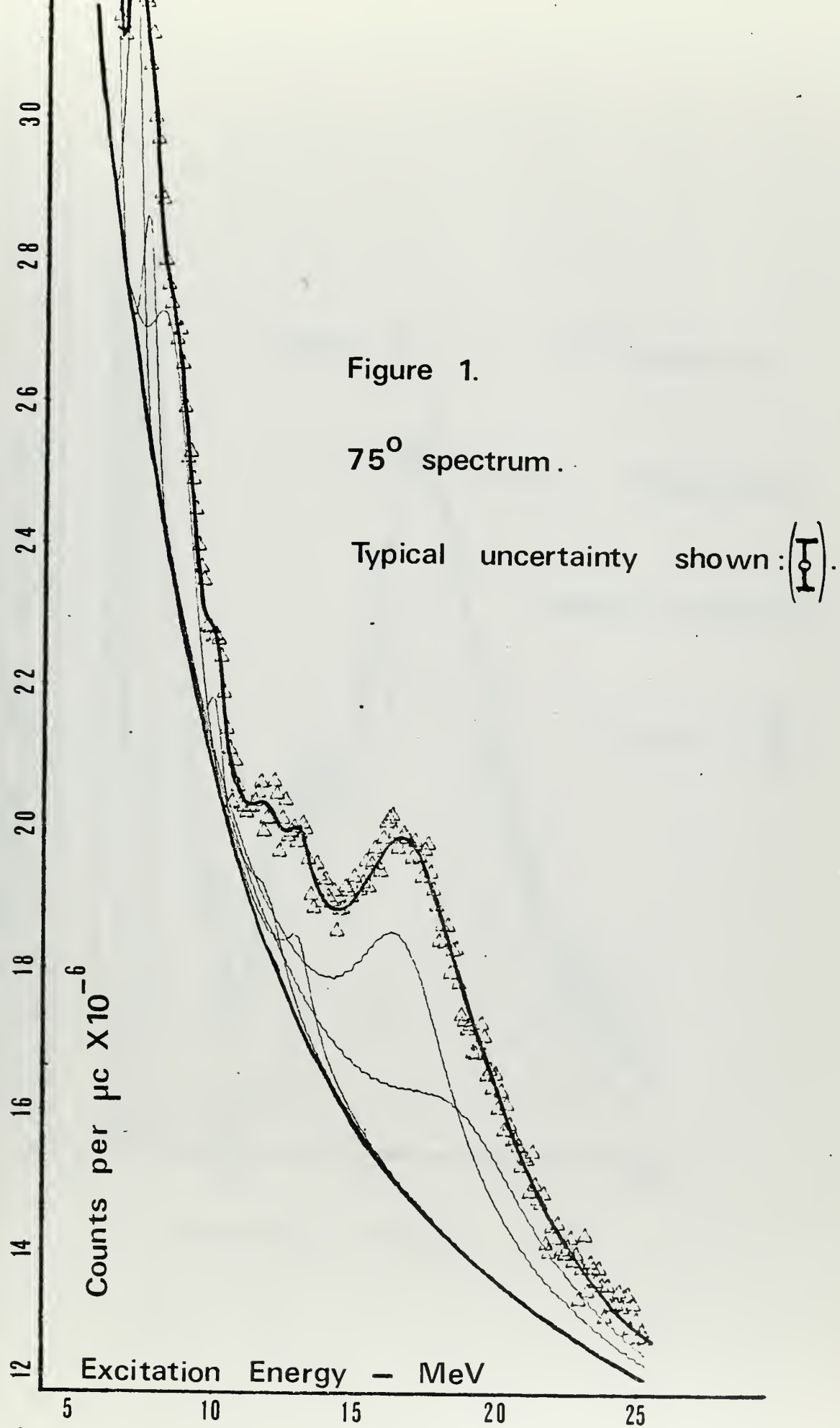E3 resonances could be M2.

TABLE IV REDUCED TRANSITION PROBABILITIES AND SUM RULES
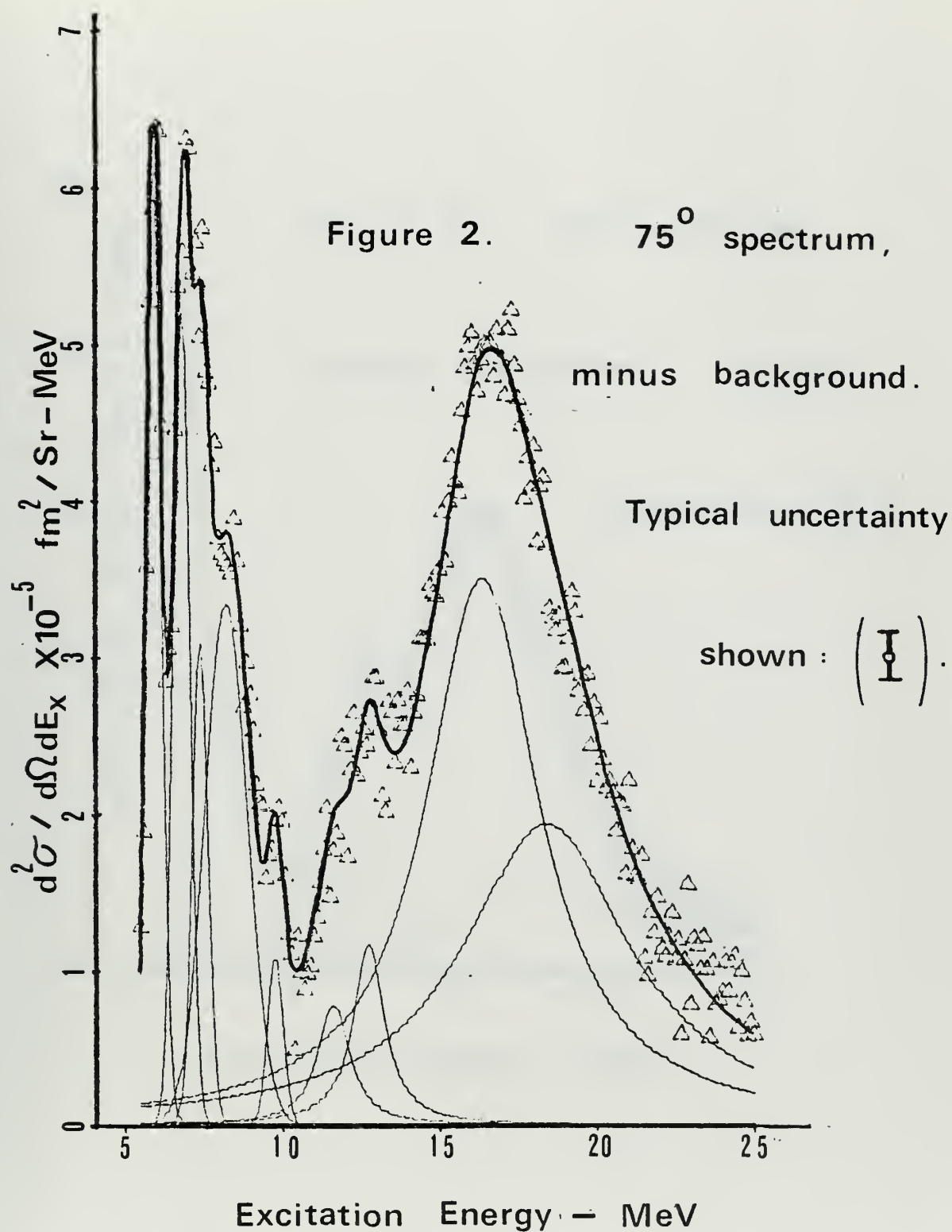(BEST χ^2 FIT ANALYSIS)

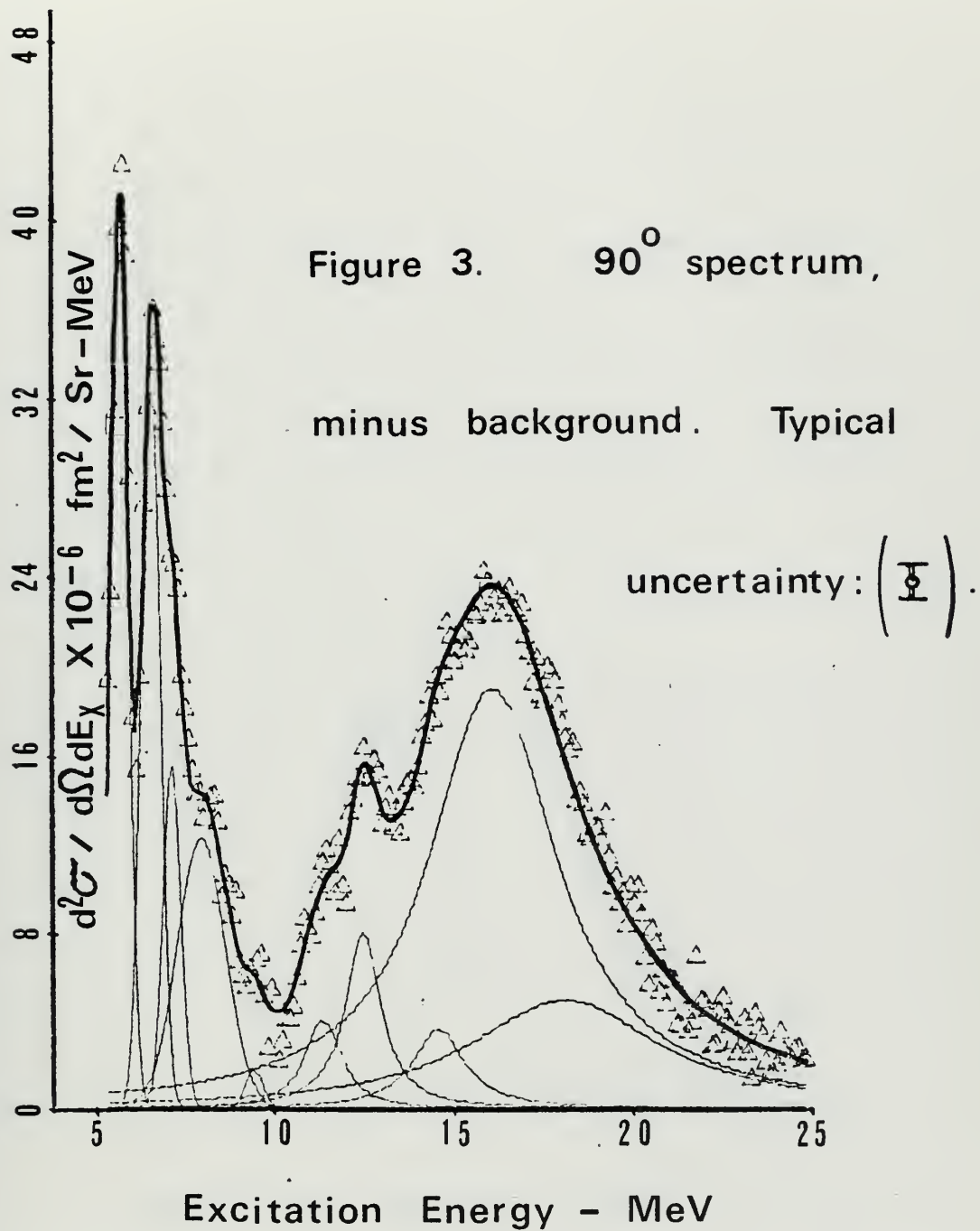| E_x Mev	λ	Γ (MeV)	ERROR (MeV)	$\bar{B}_{calc}$ (fm$^{2\lambda}$)	ERROR (fm$^{2\lambda}$)	Strength in SPU	% EWSR Dissipated
6.15 ± .04	E2	.518	.006	1.68×10^2	3.08×10^1	5.45	7.2
	E3			1.19×10^4	2.67×10^3	4.46	8.9
7.02 ± .04	E3	.595	.019	1.21×10^4	1.75×10^3	6.9	10.4
7.59 ± .02	E2	.677	.081	9.01×10^1	2.13×10^1	4.2	4.8
	E3			6.69×10^3	1.23×10^3	5.4	6.2
8.43 ± .04	E2	1.93	.26	2.43×10^2	4.26×10^1	5.7	14.3
9.90 ± .14	UNK	.997	1.0	-	-	-	-
11.8 ±..06	E4	1.31	.25	7.21×10^5	1.21×10^5	5.96	18.0
12.9 ± .02	E3	1.24	.13	5.67×10^3	3.28×10^2	17.3	9.0
14.9 ± .08	E4	2.24	.51	9.04×10^5	1.29×10^5	7.0	28.4
16.5 ± .14	E3	5.16	1.27	7.58×10^4	1.25×10^4	6.1	153.
18.5 ± .00	E1	5.74	.39	6.97	3.97×10^{-1}	17.56	58.6

TABLE V WEISSKOPF SINGLE PARTICLE UNITS AND ENERGY
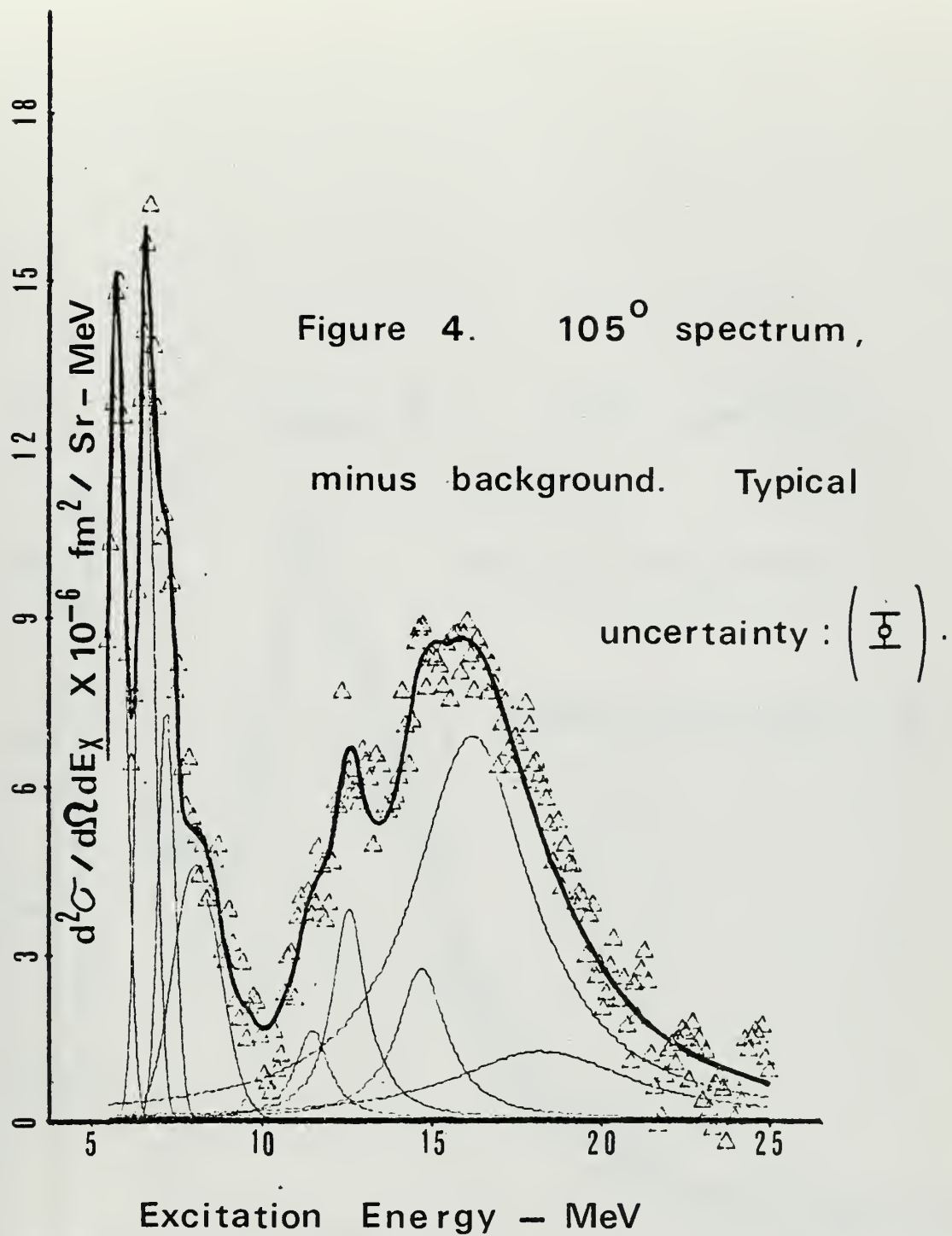WEIGHTED SUM RULES

$E\lambda$	$B(E\lambda) \frac{fm^{2\lambda}}{SPU}$	*EWSR MeV $fm^{2\lambda}$
E1	1.375	2.20×10^{2}
E2	2.52×10^{1}	1.43×10^{4}
E3	5.75×10^{2}	8.17×10^{5}
E4	1.68×10^{4}	4.73×10^{7}

*All EWSR's are isoscalar ($\Delta T=0$)

Figure 1.

75° spectrum.

Typical uncertainty shown :

Counts per μc X10⁻⁶

Excitation Energy — MeV

55

Figure 2. 75° spectrum, minus background. Typical uncertainty shown : $\left(\text{I} \right)$.

Figure 3. 90° spectrum, minus background. Typical uncertainty: $\left(\begin{array}{c} \\ \end{array} \right)$.

Figure 4. 105° spectrum, minus background. Typical uncertainty : $\left(\;\overline{\underline{\mathrm{I}}}\;\right)$.

Excitation Energy — MeV

Figure 5.   60° spectrum, minus background.

Typical uncertainty: ⌈ ⌉.

y-axis: $d^2\sigma / d\Omega dE_\chi \times 10^{-5}$ fm^2 / Sr−MeV

x-axis: Excitation Energy − MeV

FIGURE 6. Experimental inelastic form
factors for state at ― MeV

60
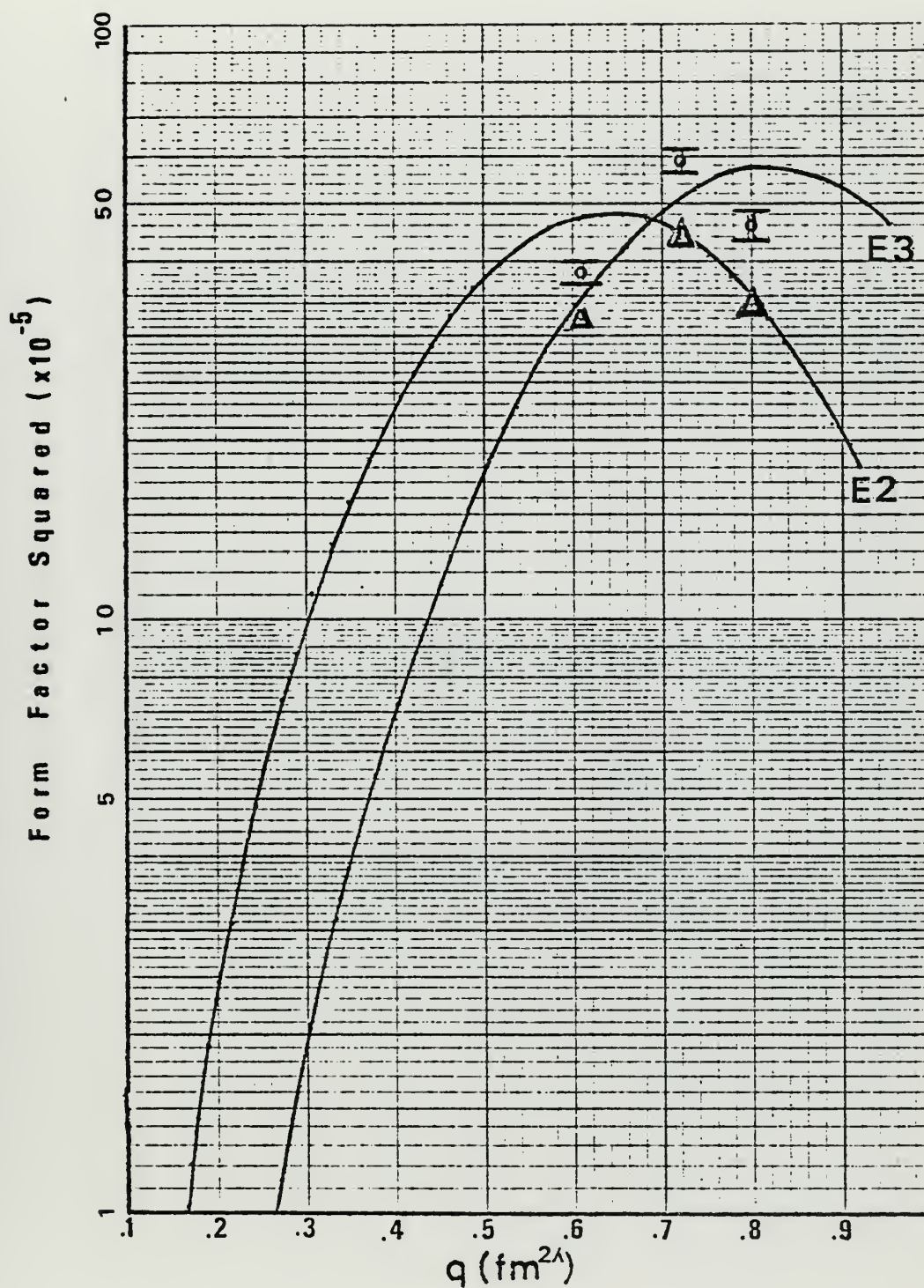
FIGURE 7. Experimental inelastic form
factors for state at 6.14 MeV

△ best x^2
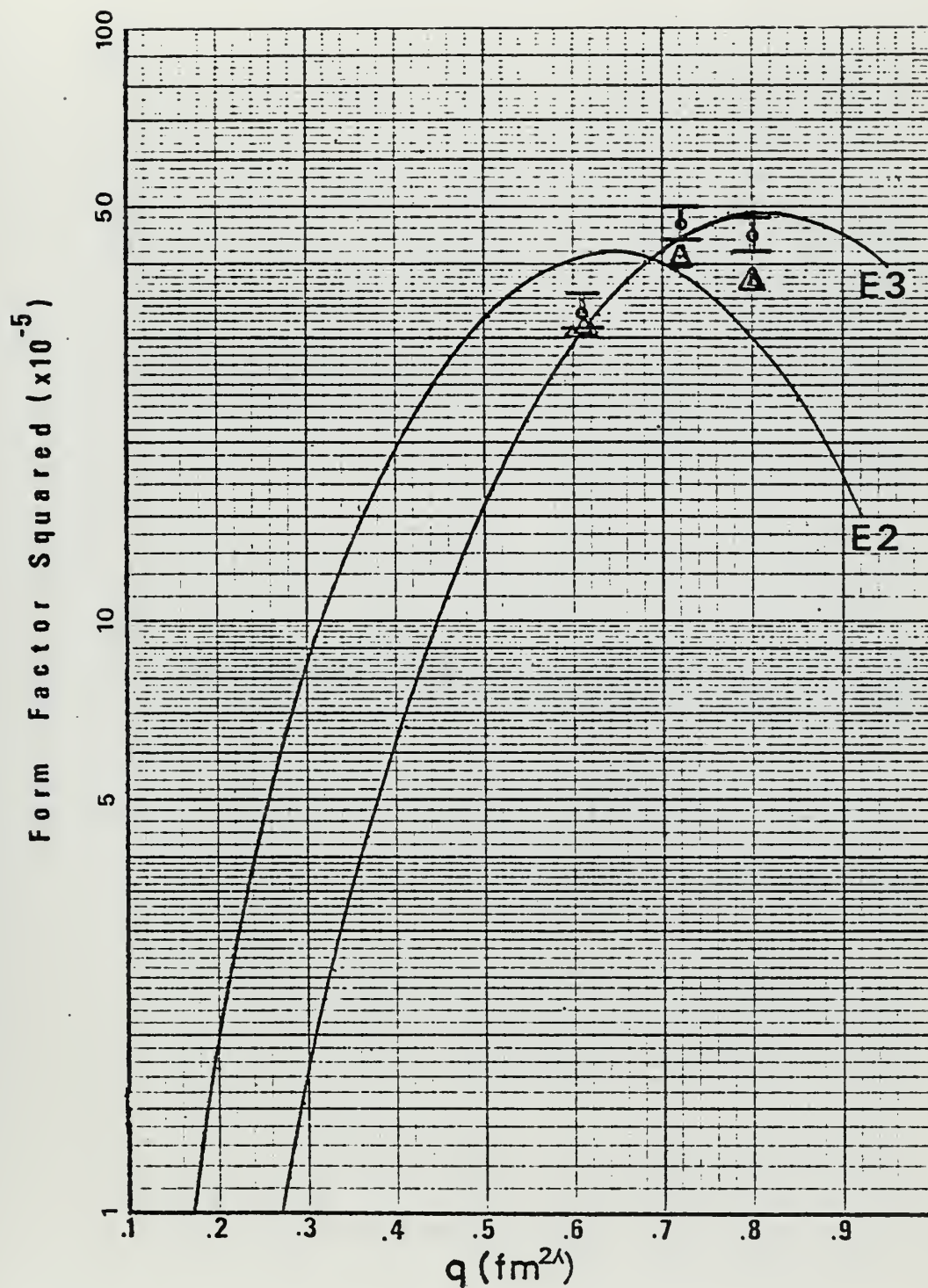
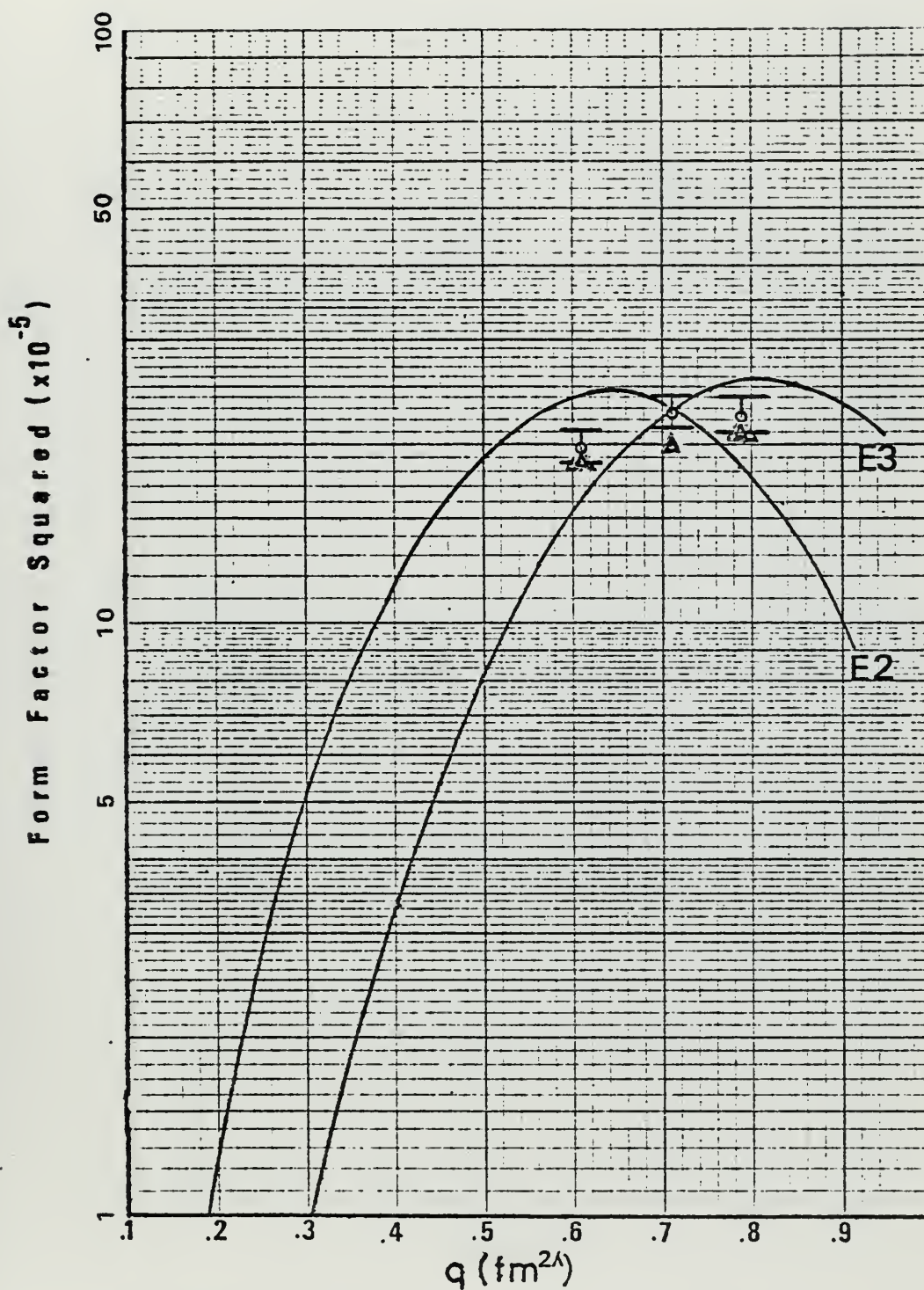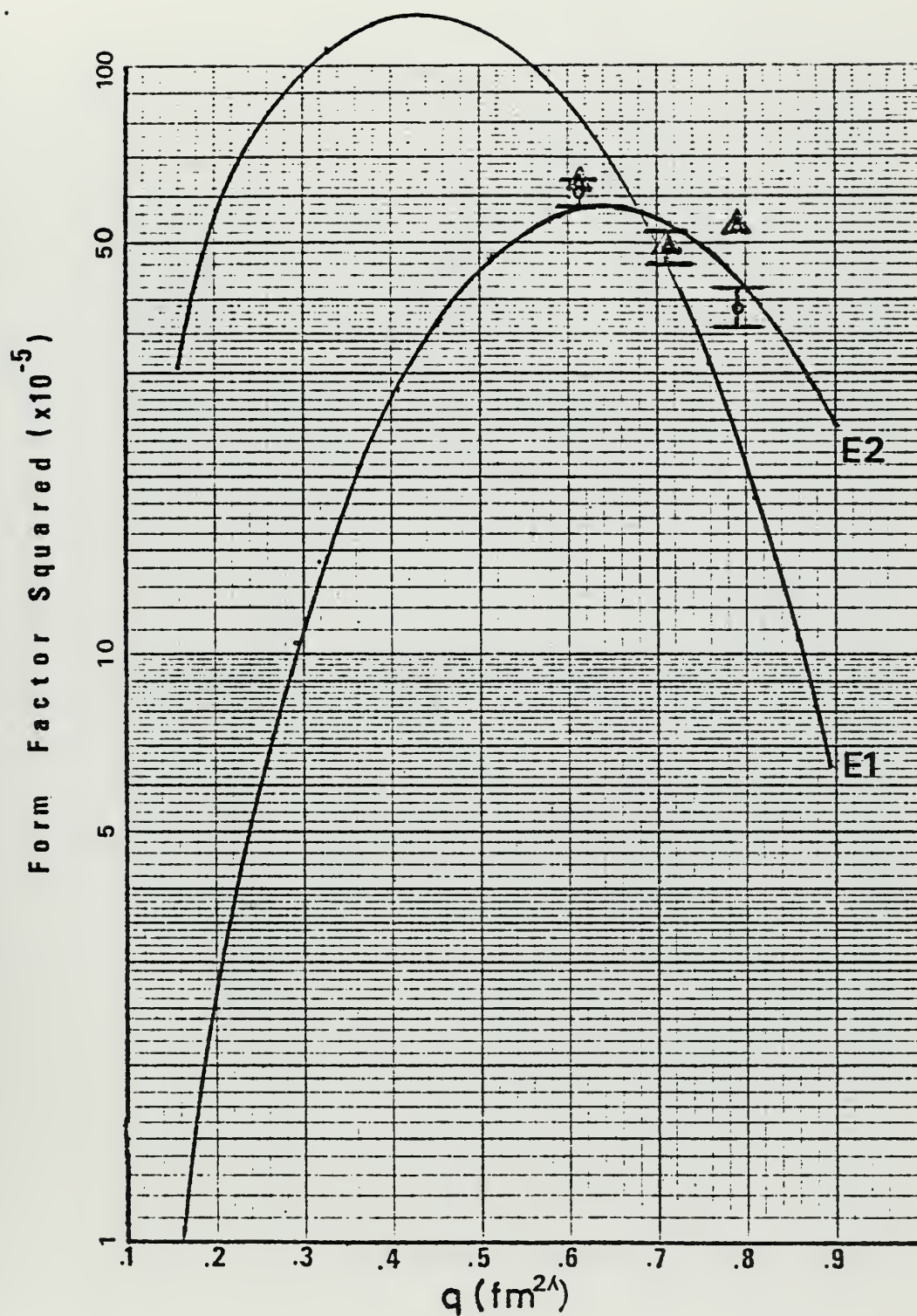FIGURE 8. Experimental inelastic form
factors for state at 7.0 MeV

Δ best x^2

FIGURE 9.   Experimental inelastic form
factors for state at 7.6   MeV
$\triangle$ best x^2

FIGURE 10. Experimental inelastic form factors for state at 8.4 MeV

△ best x^2

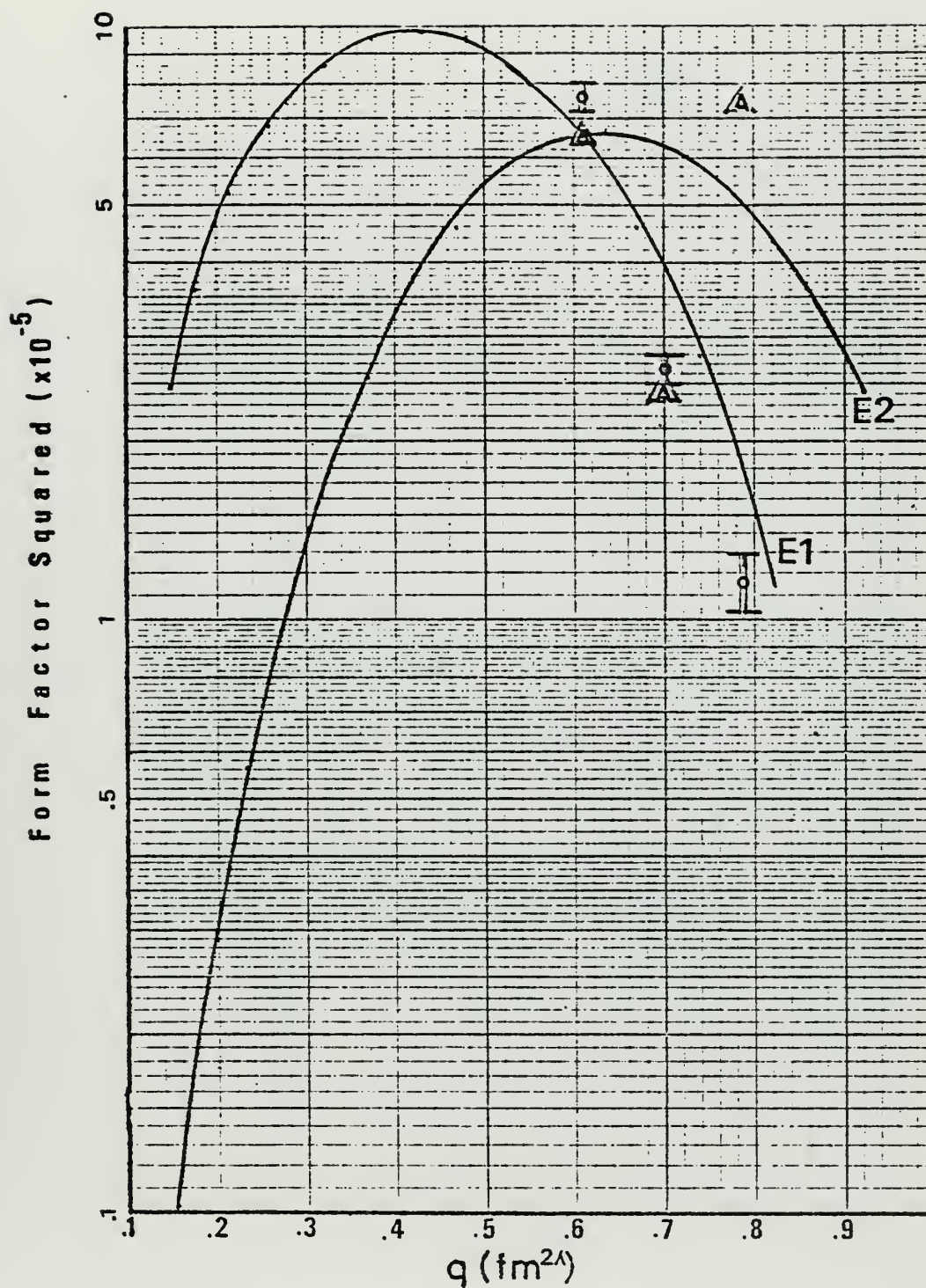Form Factor Squared ($\times 10^{-5}$)

q ($fm^{2\wedge}$)

E2

E1

FIGURE 11. Experimental inelastic form factors for state at 9.9 MeV
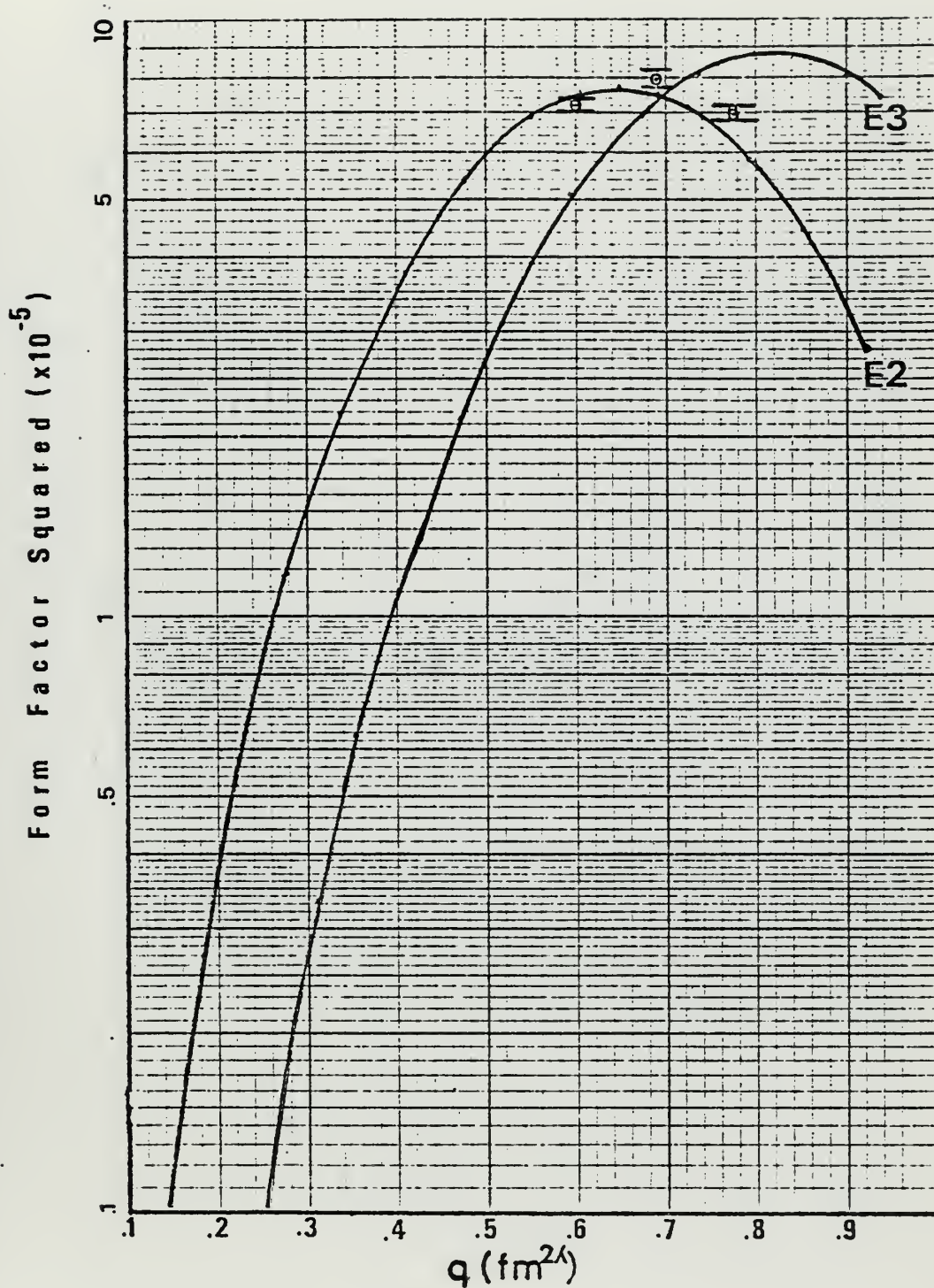
△ best X^2

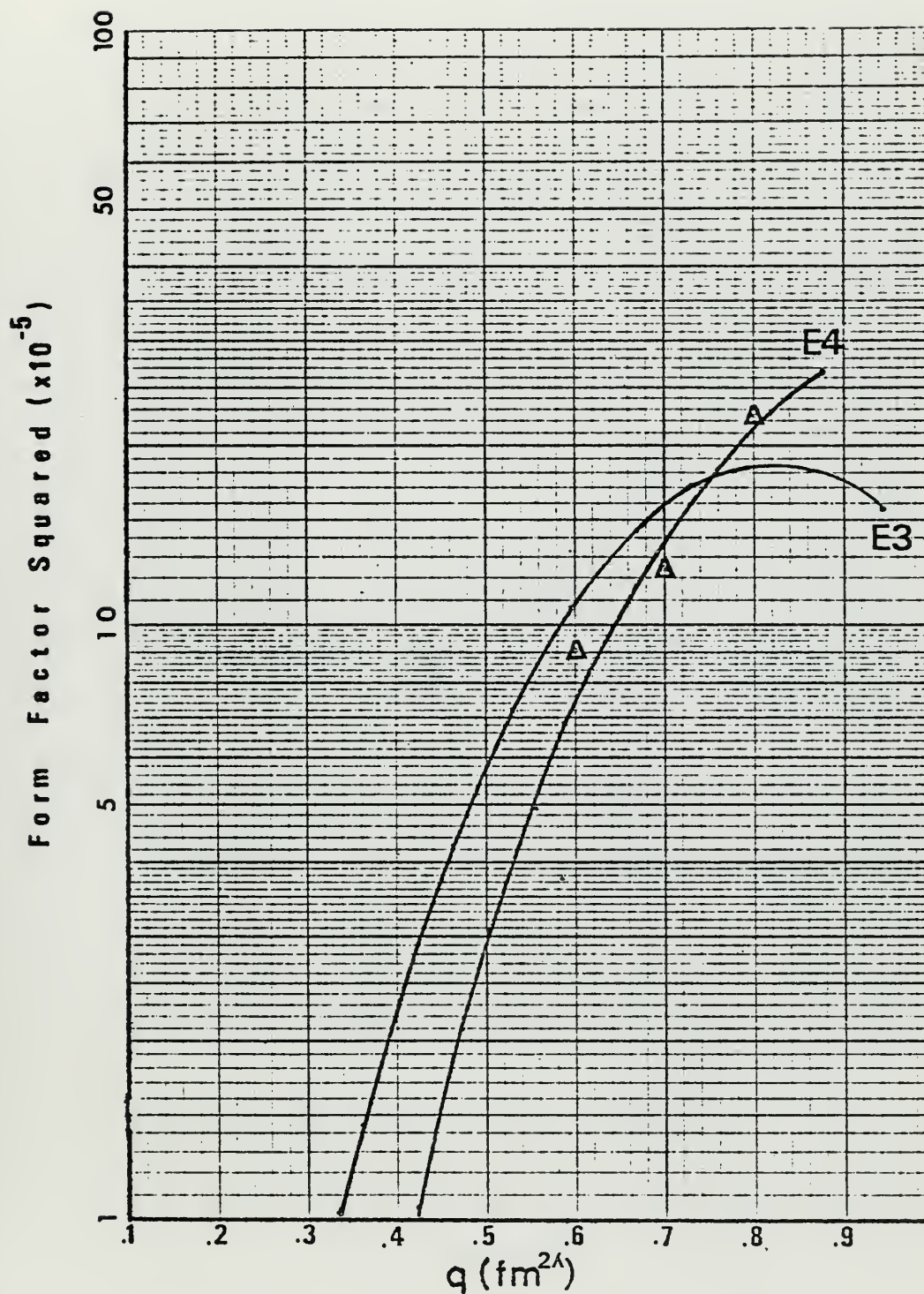FIGURE 12. Experimental inelastic form factors for state at 11.8 MeV

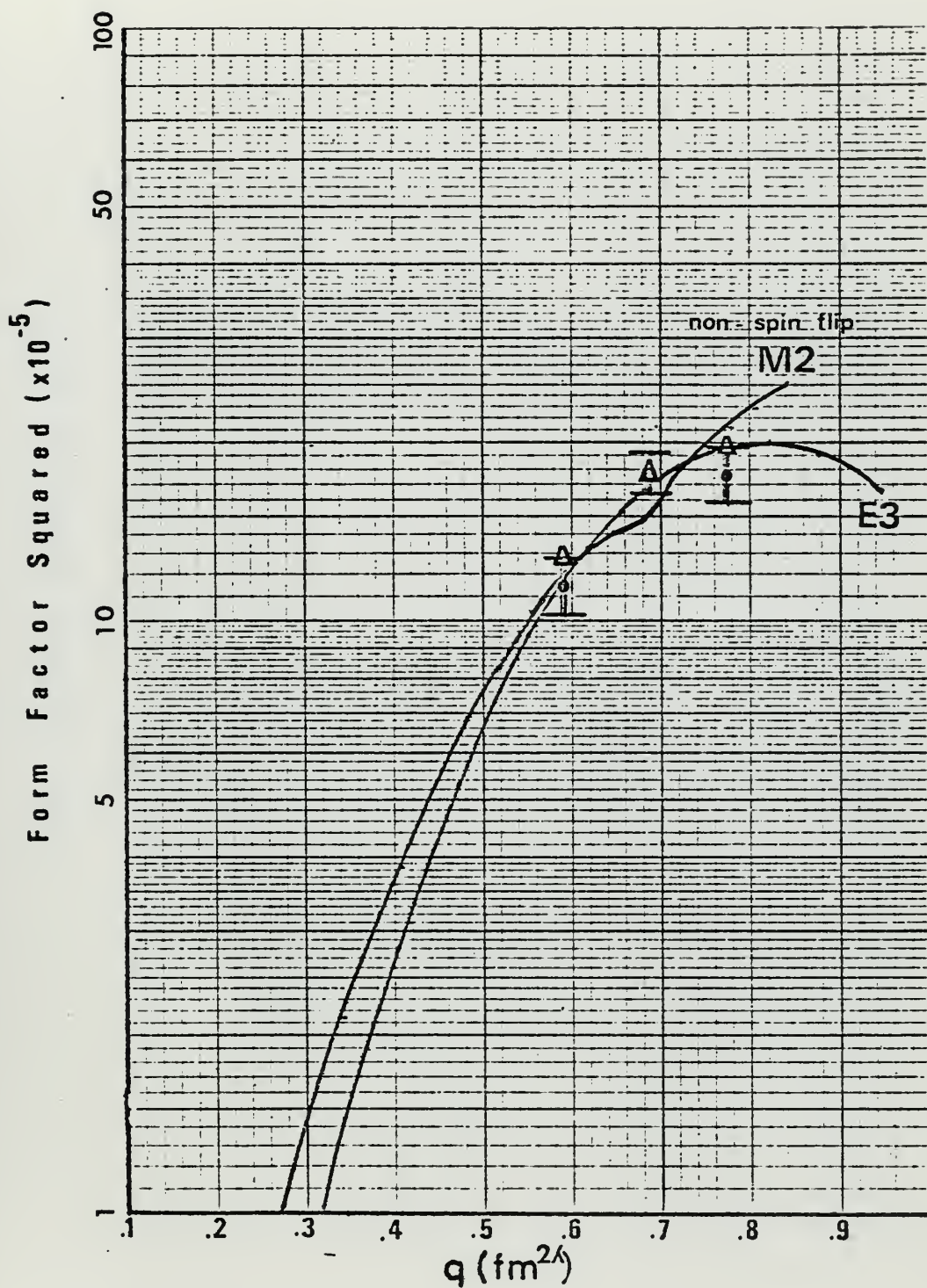FIGURE 13. Experimental inelastic form factors for state at 11.8 MeV best x^2 fit

FIGURE 14. Experimental inelastic form factors for state at 12.9 MeV

▲ best x^2

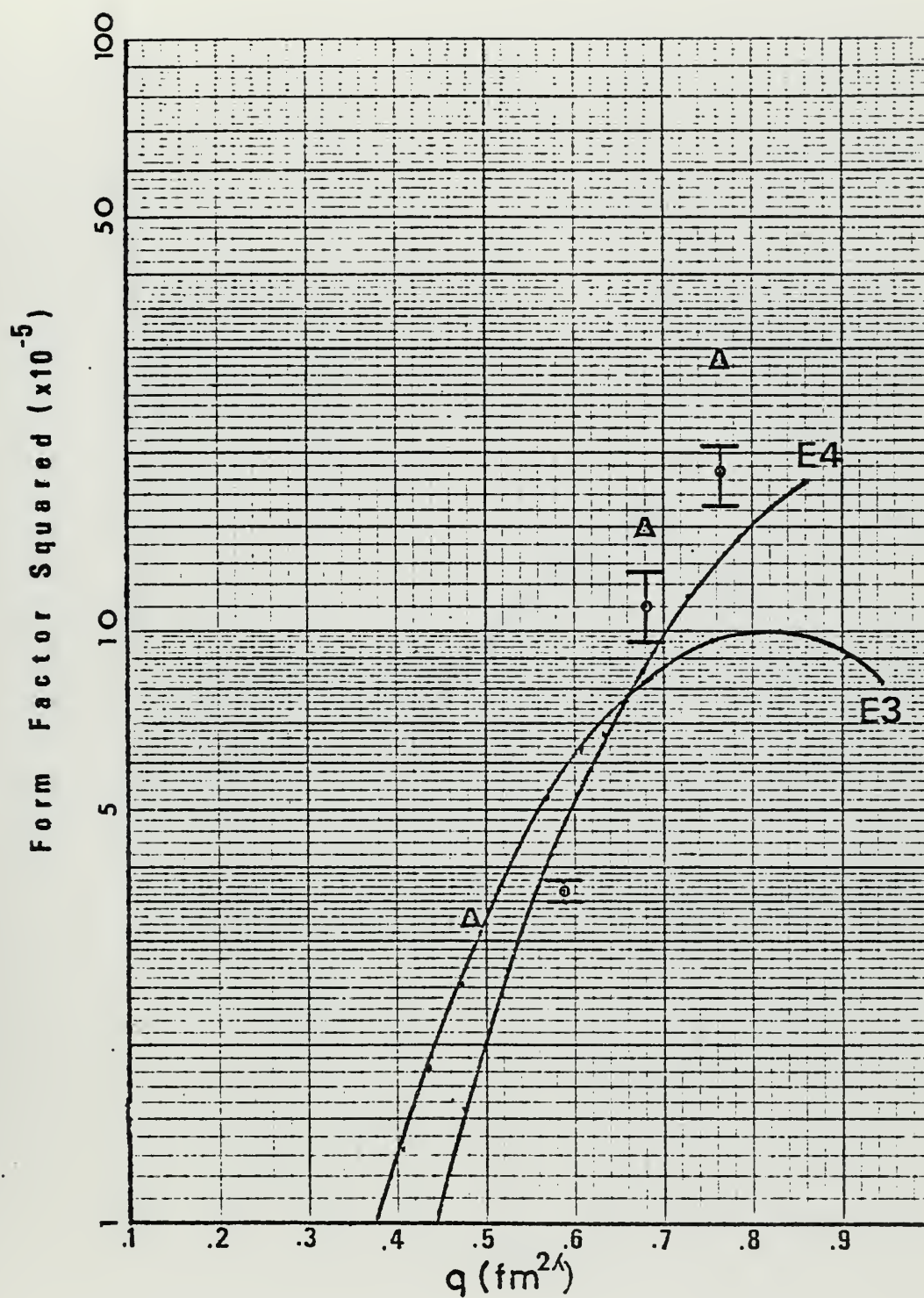FIGURE 15. Experimental inelastic form
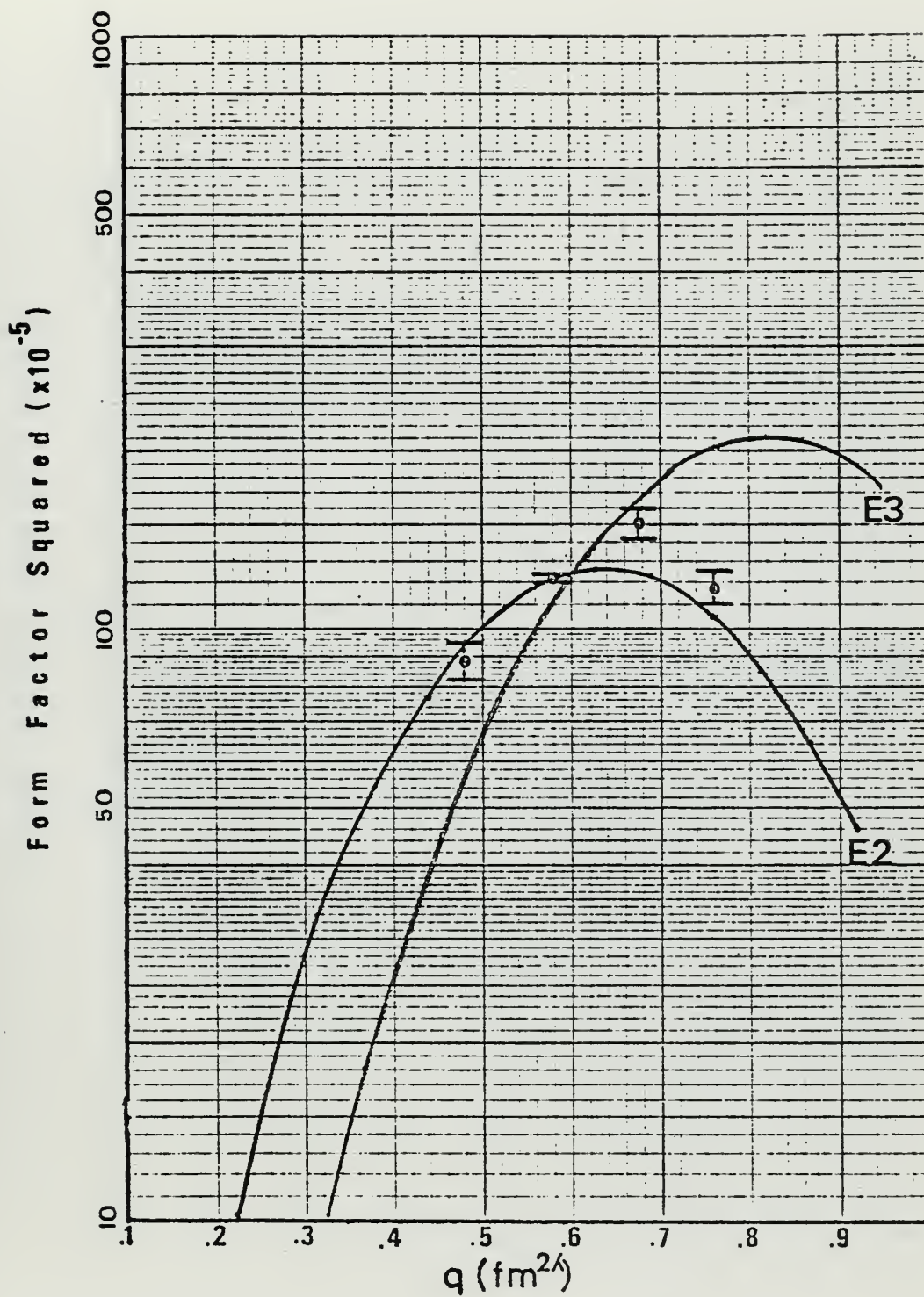factors for state at 15.0 MeV
$\triangle$ best x^2

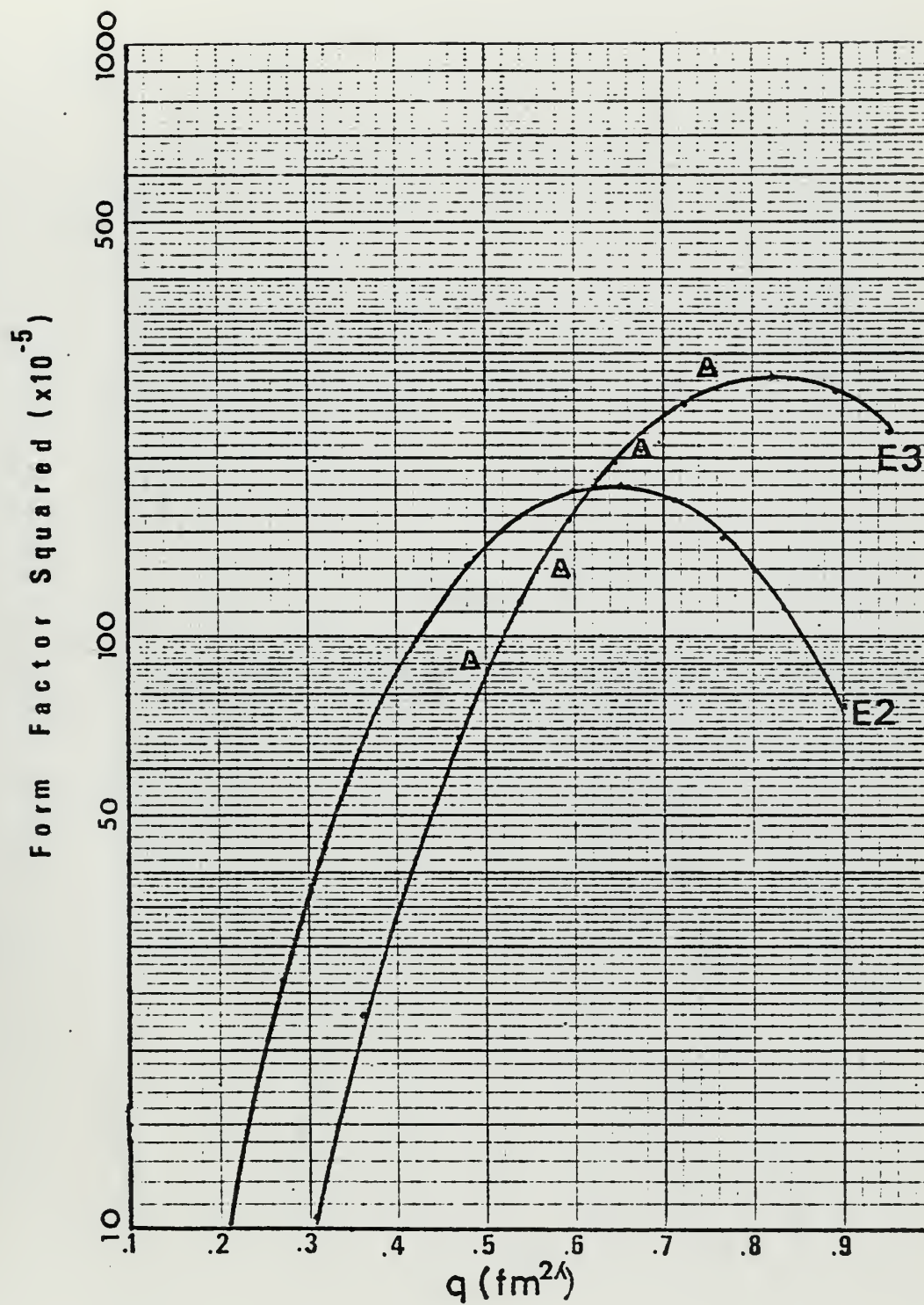FIGURE 16. Experimental inelastic form factors for state at 16.5 MeV

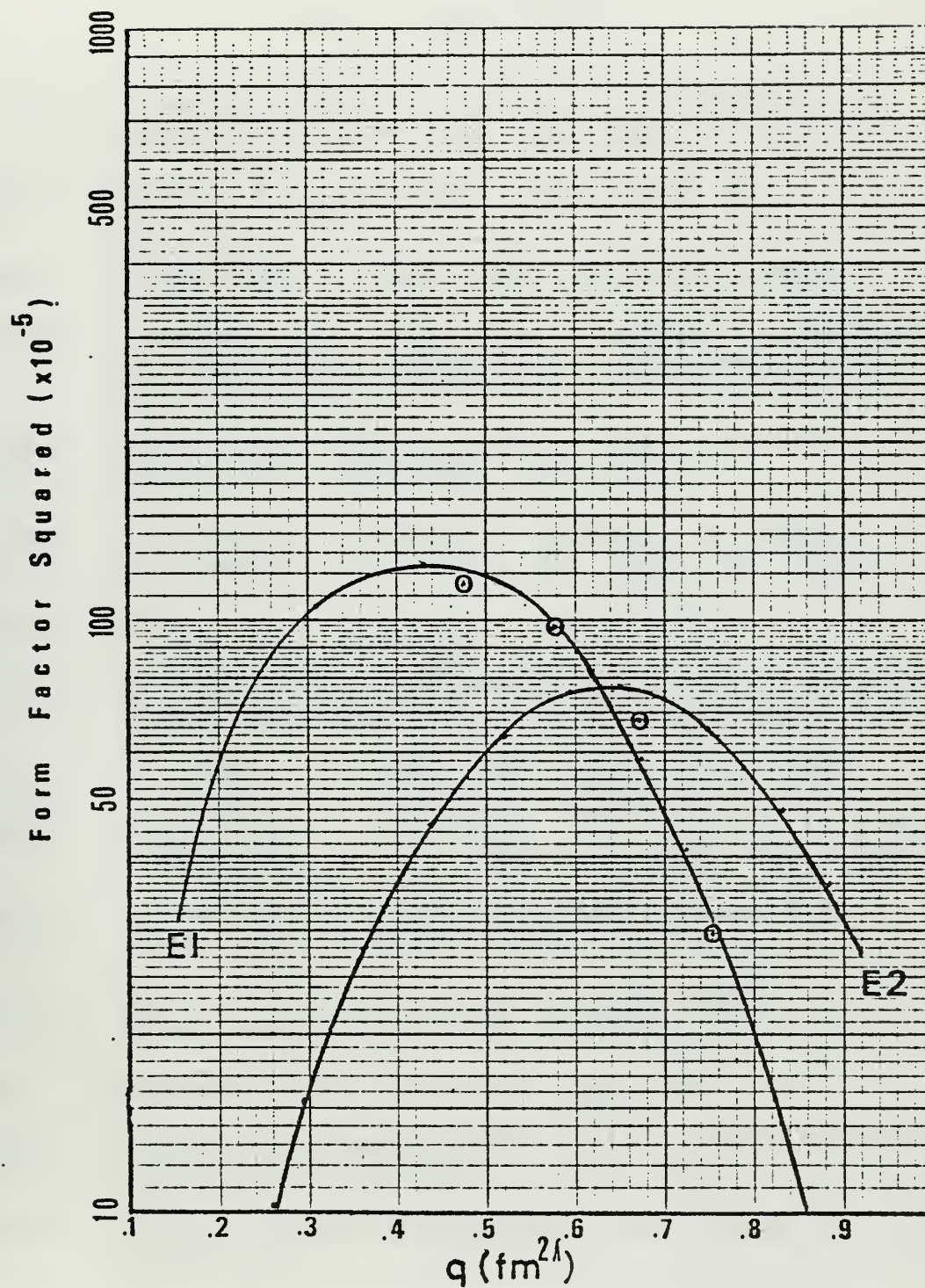FIGURE 17. Experimental inelastic form
factors for state at 16.5 MeV

best χ^2 fit

FIGURE 18. Experimental inelastic form
factors for state at 18.5 MeV

72

LIST OF REFERENCES

AdlB56   Adler, K., Bohr, A., Hans, T., Mottelson, B.,
          Winther, A.: Rev. Mod. Phys. 28, 432 (1956).

BerF75   Berman, B.L. and Fultz, S.C., Rev. Mod. Phys,
          47, 713 (1975).

Bro63   Broek, H.W.: Phys. Rev. 130, 1914 (1963).

BusG72   Buskirk, F.R., Gräf, H.D., Pitthan, R., Theissen,
          H., Titze, O., Walcher, T.: Phys. Rev. Lett.,
          42B, 194 (1972).

ChaB75   Chang, C.C., Bertrand, F.E. and Kocher, D.C.:
          Phys. Rev. Letters 34, 221 (1975).

CraH61   Crannell, H., Helm, R., Kendall, H., Oeser, J.
          and Yearian, M.: Phys. Rev. 123, 923 (1961).

Dan58   Danos, M.: Nucl. Phys. 5, 23 (1958).

deJd74   deJager, C.W., deVries, H. and deVries, C.:
          Atomic Data and Nuclear Data Tables 14, 479 (1974).

Dre68   Drechsel, D.: Nucl. Phys. A113, 665 (1968).

DugB67   Dugnay, M.A., Bockelman, C.K., Curtis, T.H. and
          Eisenstein, R.A.: Phys. Rev. 163, 1259 (1967).

Eccl66   Eccles, S.F., Lutz, H.F., and Madsen, V.A.:
          Phys. Rev. 141, 1067 (1966).

FalG65   Fallieros, S., Goulard, B., and Venter, R.H.:
          Phys. Lett. 19, 5, 398, (1965).

Fer57   Ferrell, R.A.: Phys. Rev. 101, 1631 (1957).

FerW74   Ferlic, K.P. and Waddell, R.D.: Naval Postgraduate
          School Thesis (1974).

FriS65   Fricke, M.P. and Satchler, G.R.: Phys. Rev. 139,
          B567 (1965).

FukT72   Fukuda, S. and Torizuka, Y.: Phys. Rev. Lett.
          29, 1109 (1972).

FulA74   Fultz, S.C., Alvarez, R.A., Berman, B.L., and
          Meyer, P.: Phys. Rev. 10, 608 (1974).

GolT8   Goldhaber, M. and Teller, E.: Phys. Rev. 74,
           1046 (1948).

Gul71   Gul'Karov, I.S.: Soviet Journal of Nuclear Physics
           13, 178 (1971).

Gul73   Gul'Karov, I.S.: Soviet Journal of Nuclear Physics
           18, 267 (1973).

GulA69   Gul'Karov, I.S., Afanas'Ev, N.G., Khvastunov, V.M.,
           Shevchenko, N.G., Afanas'Ev, V.D., Savitskii, G.A.
           and Khomich, A.A.: Soviet Journal of Nuclear Physics
           9, 274 (1969).

Hay69   Hayward, E., Photonuclear Reactions, Physics Part
           IV Lecture Notes. School of Physics, University of
           Melbourne, Australia (1969).

IsaB63   Isabelle, D.B., and Bishop, G.R.: Nucl. Phys. 45,
           209 (1963).

Jol65   Jolly, R.K.: Phys. Rev. 139, B318 (1965).

KocB73   Kocher, D.C., Bertrand, F.E., Gross, E.E., Lord, R.S.
           and Newman, E.: Phys. Rev. Lett. 31, 1070 (1973).

Mig44   Migdal, A.: J. Phys. USSR 8, 331 (1944).

MoaB73   Moalem, A., Benenson, W. and Crawley, G.W.: Phys.
           Rev. Lett. 31, 482 (1973).

MohP65   Mohindra, R.K. and VanPatter, D.M.: Phys. Rev.
           139, B274 (1965).

Moo74   Moore, G.L. Naval Postgraduate School Thesis (1974).

Mot29   Mott, N.F., Proc. Roy. Soc. (London) A124, 425
           (1929), as reprinted in Hofstader, R., Electron
           Scattering and Nuclear Structure, Benjamin, New
           York (1963).

NatN66   Nathan, O. and Nilsson, S.G., in Alpha, Beta, and
           Gamma-ray Spectroscopy, ed. by K. Siegbahn, North-
           Holland Publishing Company, Amsterdam (1966).

Pit73   Pitthan, R. , Dissertation, Institut für Kernphysik
           der Technische Hochschule Darmstadt (1972):
           unpublished.

PitB74   Pitthan, R. , Buskirk, F.R., Dalley, E.B., Dyer,
           J.N., Maruyama, X.K.: Phys. Rev. Lett. 33, 849,
           (1974).

PitW71   Pitthan, R. and Walcher, T.:   Phys. Rev. Lett.
          36B, 563 (1971).

SkoH66   Skorka, S.J., Hertel, J., Retz-Schmidt, T.W.,
          Nucl. Data A2, 347 (1966).

SteJ50   Steinwedel, H. and Jensen, J.H.D., Z. Naturforsch.
          a5, 413 (1950).

INITIAL DISTRIBUTION LIST

No. Copies

1. Defense Documentation Center   2
   Cameron Station
   Alexandria, Virginia 22314

2. Library, Code 0212   2
   Naval Postgraduate School
   Monterey, California 93940

3. Department Chairman, Code 61   2
   Department of Physics and Chemistry
   Naval Postgraduate School
   Monterey, California 93940

4. Assoc. Professor E.B. Dally, Code 61 Dy   3
   Department of Physics and Chemistry
   Naval Postgraduate School
   Monterey, California 93940

5. Professor W.R. Pitthan, Code 61Pt   3
   Department of Physics and Chemistry
   Naval Postgraduate School
   Monterey, California 93940

6. Professor F.R. Buskirk, Code 61Bs   3
   Department of Physics and Chemistry
   Naval Postgraduate School
   Monterey, California 93940

7. LCDR D.H. DuBois II, USN   2
   12740 Old Spanish Trail
   San Antonio, Texas 78233

8. LCDR G.M. Bates, USN   2
   USS Wainwright (CG-28)
   FPO New York, New York 09501